

UCSF

UC San Francisco Previously Published Works

Title

Kinetic analysis of Cas12a and Cas13a RNA-Guided nucleases for development of improved CRISPR-Based diagnostics

Permalink

<https://escholarship.org/uc/item/7bm344gq>

Journal

iScience, 24(9)

ISSN

2589-0042

Authors

Nalefski, Eric A
Patel, Nidhi
Leung, Philip JY
et al.

Publication Date

2021-09-01

DOI

10.1016/j.isci.2021.102996

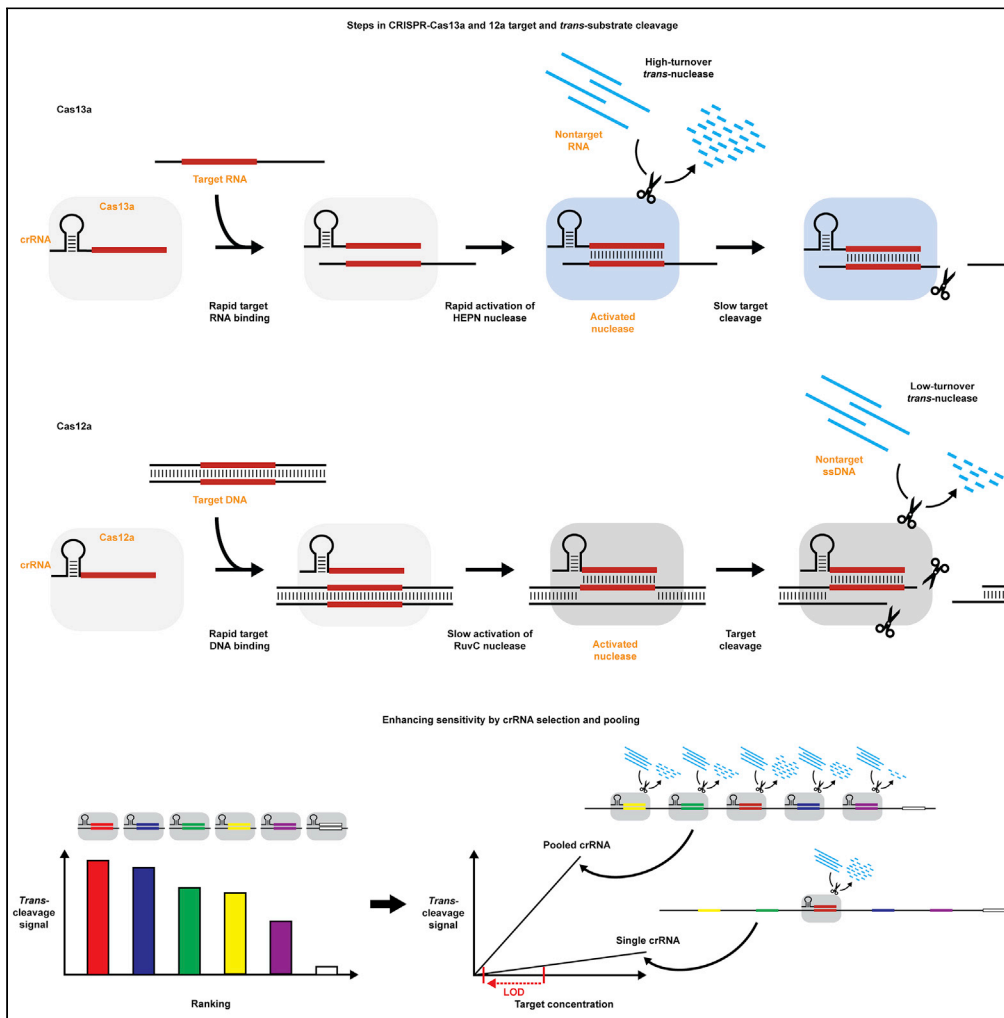
Copyright Information

This work is made available under the terms of a Creative Commons Attribution License, available at <https://creativecommons.org/licenses/by/4.0/>

Peer reviewed

Article

Kinetic analysis of Cas12a and Cas13a RNA-Guided nucleases for development of improved CRISPR-Based diagnostics



Eric A. Nalefski, Nidhi Patel, Philip J.Y. Leung, ..., Jennifer A. Doudna, Anne-Laure M. Le Ny, Damian Madan

eric.nalefski@ghlabs.org (E.A.N.)
damian.madan@ghlabs.org (D.M.)

Highlights

Cas13a HEPN trans-RNase activation is directly coupled to rapid target RNA binding

Cas12a RuvC trans-nuclease activity is coupled to slow target DNA cleavage

Individual crRNA generate widely varying levels of targeted trans-cleavage

Pooling multiple crRNA allows pathogen quantification without target amplification

Nalefski et al., iScience 24, 102996
September 24, 2021 © 2021 The Authors.
<https://doi.org/10.1016/j.isci.2021.102996>



Article

Kinetic analysis of Cas12a and Cas13a RNA-Guided nucleases for development of improved CRISPR-Based diagnostics

Eric A. Nalefski,^{1,2,*} Nidhi Patel,¹ Philip J.Y. Leung,^{1,2} Zeba Islam,¹ Remy M. Kooistra,^{1,2} Ishira Parikh,¹ Estelle Marion,³ Gavin J. Knott,^{4,5,6} Jennifer A. Doudna,^{4,6,7,8,9,10} Anne-Laure M. Le Ny,^{1,2} and Damian Madan^{1,2,11,*}

SUMMARY

Bacterial CRISPR systems provide acquired immunity against invading nucleic acids by activating RNA-programmable RNases and DNases. Cas13a and Cas12a enzymes bound to CRISPR RNA (crRNA) recognize specific nucleic acid targets, initiating cleavage of the targets as well as non-target (*trans*) nucleic acids. Here, we examine the kinetics of single-turnover target and multi-turnover *trans*-nuclease activities of both enzymes. High-turnover, non-specific Cas13a *trans*-RNase activity is coupled to rapid binding of target RNA. By contrast, low-turnover Cas12a *trans*-nuclease activity is coupled to relatively slow cleavage of target DNA, selective for DNA over RNA, indifferent to base identity, and preferential for single-stranded substrates. Combining multiple crRNA increases detection sensitivity of targets, an approach we use to quantify pathogen DNA in samples from patients suspected of Buruli ulcer disease. Results reveal that these enzymes are kinetically adapted to play distinct roles in bacterial adaptive immunity and show how kinetic analysis can be applied to CRISPR-based diagnostics.

INTRODUCTION

CRISPR-Cas systems provide bacteria and archaea acquired immunity using programmable crRNA to guide nuclease activity against viruses and plasmids. CRISPR-Cas systems are divided into six types by identity and architecture of protein domains, types of nucleic acid polymers they cleave, and mechanisms by which cleavage is catalyzed (Koonin et al., 2017). Cas12a, of the large, diverse type V family (Yan et al., 2019), binds crRNA to form ribonucleoproteins (RNP) that cleave single-stranded (ss) as well as double-stranded (ds) DNA targets containing sequences complementary to the crRNA (Zetsche et al., 2015). This engagement also activates non-specific cleavage of ssDNA, ssRNA, and dsDNA (Chen et al., 2017; Fu et al., 2019; Fuchs et al., 2019; Li et al., 2018; Murugan et al., 2020). Cas13a, a type VI enzyme (Shmakov et al., 2015), binds crRNA to form RNP that cleave specific RNA targets; this interaction activates robust non-specific cleavage of RNA (Abudayyeh et al., 2015; East-Seletsky et al., 2016). Though mechanisms have been proposed, the roles of Cas12a-mediated and Cas13a-mediated *trans*-activity in viral defense remain incompletely understood (Varble and Marraffini, 2019).

Upon crRNA-targeted binding of Cas12a to protospacers juxtaposed to consensus protospacer adjacent motifs (PAM) that mark targets as foreign, DNA strands within the protospacer are separated—leading to hybridization of the crRNA spacer to the displaced target strand (TS) to form an R-loop structure—followed by cleavage of the two strands. Cas12a RuvC-like nuclease first cleaves the separated non-target strand (NTS) in the R-loop within the protospacer 18-nt from the PAM via a proposed two-metal ion mechanism, which leads to further denaturation of protospacer strands beyond the PAM-proximal ends of the R-loop and cleavage of the separated TS outside the protospacer (Cofsky et al., 2020; Stella et al., 2018). The cleaved PAM-proximal fragments dissociate very slowly, effectively limiting Cas12a to single-turnover of targets (Singh et al., 2018; Sternberg et al., 2014) but allowing multiple rounds of additional cleavage of non-target nucleic acids supplied in *trans* (Chen et al., 2017; Li et al., 2018). Likewise, in Cas13a, hybridization of crRNA to target RNA allosterically activates conformational changes, bringing together two HEPN domains to form a composite catalytic site that cleaves both target RNA as well non-target ssRNA in a

¹Global Health Labs, Bellevue, WA 98007, USA

²Center for In Vitro Diagnostics, Intellectual Ventures Global Good Fund, Bellevue, WA 98007, USA

³Inserm, Université d'Angers, Angers, France

⁴Department of Molecular and Cell Biology, University of California, Berkeley, Berkeley, CA 94704, USA

⁵Monash Biomedicine Discovery Institute, Department of Chemistry & Molecular Biology, Monash University, Melbourne, VIC 3800, Australia

⁶Innovative Genomics Institute, University of California, Berkeley, Berkeley, CA 94720, USA

⁷MBIB Division, Lawrence Berkeley National Laboratory, Berkeley, CA 94720, USA

⁸Department of Chemistry, University of California, Berkeley, Berkeley, CA 94704, USA

⁹Howard Hughes Medical Institute, University of California, Berkeley, Berkeley, CA 94704, USA

¹⁰Gladstone Institute of Data Science and Biotechnology, Gladstone Institutes, San Francisco, CA 94158, USA

¹¹Lead contact

*Correspondence: eric.nalefski@ghlabs.org (E.A.N.), damian.madan@ghlabs.org (D.M.)

<https://doi.org/10.1016/j.isci.2021.102996>



divalent cation-dependent manner (Abudayyeh et al., 2015; East-Seletsky et al., 2016, 2017). Though much is known about target sequence requirements and steps leading to cleavage of targets by Cas12a and Cas13a, steps critical for activation of downstream effector nuclease activities are relatively uncharacterized.

The explosion of reports using Cas12a and Cas13a to detect various nucleic acid sequences indicates their potential as powerful new diagnostic tools (Li et al., 2019). To date, certain biochemical properties have prevented them from reaching their full potential in field-deployable diagnostic assays that could serve to improve global health. For instance, both appear to lack the sensitivity required to detect biologically-relevant concentrations of nucleic acids, a shortcoming typically overcome in Cas-based assays by pre-amplifying target sequences using various nucleic acid amplification techniques (NAAT). However, target amplification poses risks of carryover contamination, especially in clinical settings where assays are often run in a limited number of dedicated spaces (Aslanzadeh, 2004; Borst et al., 2004). Since high rates of false positivity are untenable for most clinical applications, commercial NAAT platforms resort to integrated design features—such as enclosed housings—to limit cross-contamination, adding to assay cost and complexity and limiting uptake, especially in low- and middle-income countries (Aslanzadeh, 2004; Bissonnette and Bergeron, 2006). Furthermore, target pre-amplification convolutes the Cas-generated quantitative response to the original target, constraining analyte detection to a binary output.

Given the central role in bacterial immunity that Cas enzymes play and their growing use in gene editing and diagnostics (Li et al., 2018, 2019), a more complete understanding of the relationship between target recognition and nuclease activities in Cas12a and Cas13a is needed. We examined substrate specificity for *trans*-nuclease activity, including the influence of length, base composition and sugar backbone, role of crRNA processing on nucleolytic activity, and temporal relationship between target engagement and triggering of nucleolytic activity. We developed a substrate-capture approach to perform endpoint and steady-state kinetic examination of single-turnover target and multi-turnover *trans*-substrate nuclease activities of crRNA-activated *Leptotrichia buccalis* Cas13a (LbuCas13a) and *Lachnospiraceae bacterium* Cas12a (LbCas12a). We used the knowledge gained to tune conditions, enabling direct, amplification-free quantification of pathogen DNA in clinical specimens. Our findings provide insight into mechanisms by which these enzymes perform nucleolytic destruction and their role in adaptive immunity and demonstrate how such analysis can guide the development of CRISPR-based diagnostics.

RESULTS

Cas13a: target cleavage and *trans*-nuclease activation

Despite the widespread use of Cas13a in diagnostic applications, relatively little is known about the kinetic properties of its HEPN RNase. We created substrate-capture assays to measure crRNA-guided nucleolytic activities of Cas enzymes against targets in *cis* and non-specific substrates in *trans* (Figure 1), whereupon cleaved products are quantified using standard curves of uncleaved substrate (Figure S1; Table S2). Cas13a target cleavage was measured using an RNA target modified by extending its 5' end with U₁₀, since uridine is the preferred substrate for this ortholog (East-Seletsky et al., 2017), internally labeling one base with a biotin capture tag and 5' end-labeling with Alexa 488 (Figure 2A). Cas13a *trans*-RNase activity was measured using polyuridine substrates labeled at opposite ends with biotin and Alexa 488 (Figure 2B). As expected, both target and *trans* cleavage required complementarity between target and crRNA and the presence of divalent cations. Cas13a also cleaved RNaseAlert (Figure S2A), widely used to record Cas13a activation, but not DNA (Figure S2B).

Target cleavage was monitored under single-turnover conditions using Cas13a RNP in excess of target: cleavage at 37°C proceeded with a first-order rate constant k_{obs} of 0.005 s⁻¹ and slowed to 0.002 s⁻¹ at 25°C (Figure S3A), the temperature chosen for further studies. Target cleavage reached a maximal rate of 0.0018 s⁻¹ as RNP concentration was raised from 2.5 to 10 nM (Figure 2C), indicating target binding to RNP achieves a rapid, non-rate-limiting equilibrium with K_d considerably <2.5 nM and cleavage just 5' to the protospacer is much slower than binding. This observed rate can be attributed to slow, post-target binding steps leading up to and including chemical rates of target cleavage. Replacing the salt-EDTA quench solution with denaturant gave similar results (Figure S3B), confirming that the assay monitors target cleavage rather than capture tag sequestration. RNP formed from precursor crRNA containing additional 6-nt 5' to the processing site cleaved target more rapidly, raising k_{obs} to 0.0028 s⁻¹ (Figure 2D), also

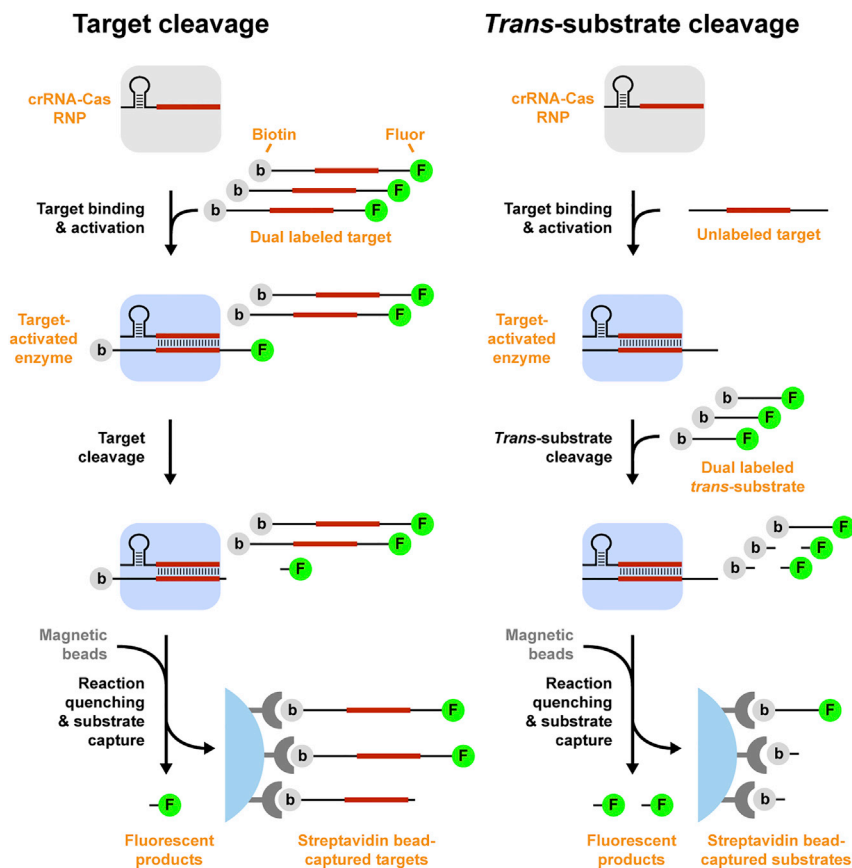


Figure 1. Substrate-capture to measure Cas nucleolytic activity

approaching a maximal rate as target concentration was raised from 0.25 to 2.0 nM (Figure 2E), confirming slow target cleavage follows rapid binding equilibrium and precursor crRNA activates a faster target RNase.

To investigate the relationship between target binding and cleavage in *cis* and activation of *trans*-RNase activity, both cleavage reactions were measured simultaneously by employing distinct fluorophores on target and *trans*-substrate (Figure 2F). Cas13a bound with mature, processed crRNA cleaved target at rates unaffected by the presence of *trans*-substrate, itself cleaved at least five-fold faster than target (k_{obs} 0.011–0.012 s^{-1}), and replacing mature with precursor crRNA again enhanced both target and *trans*-cleavage rates (Figure 2G). Extending the 5' end of dual-labeled target from U₁₀ to U₂₀ only modestly increased the target cleavage rate (k_{obs} 0.0024–0.0025 s^{-1}) and did not affect the faster *trans*-cleavage rates (Figure S3C). Together, these results demonstrate that the Cas13a RNase is rapidly activated after binding of the target, which may be cleaved more slowly than *trans*-substrates, suggesting the former is not generally required for the latter.

Cas13a: *Trans*-RNase

We explored the effect of substrate length and crRNA form on Cas13a *trans*-cleavage. The longer U₂₀ *trans*-substrate was cleaved somewhat more efficiently than shorter ones (Figure S2C). For one crRNA-target pair, direct dependence of product formation on target concentration revealed apparent turnover rates k_{app} of 0.065 s^{-1} and 0.89 s^{-1} for 10 and 100 nM U₁₀ *trans*-substrate, respectively, over 2 hr (Figure 3A), suggesting $K_M > 100$ nM and k_{cat}/K_M may be as low as $7\text{--}9 \times 10^6 \text{ M}^{-1} \text{ s}^{-1}$. Again, crRNA precursors were considerably more potent in activating targeted *trans*-cleavage than mature forms, an effect observed for several crRNA-target pairs, as well as when used to activate Cas13a K1082A (Figures 3B, 3C, and S2D–S2H; Table S3), a crRNA-processing deficient variant (East-Seletsky et al., 2017). These results indicate that higher *trans*-RNase activity resulting from crRNA precursors does not require processing to occur.

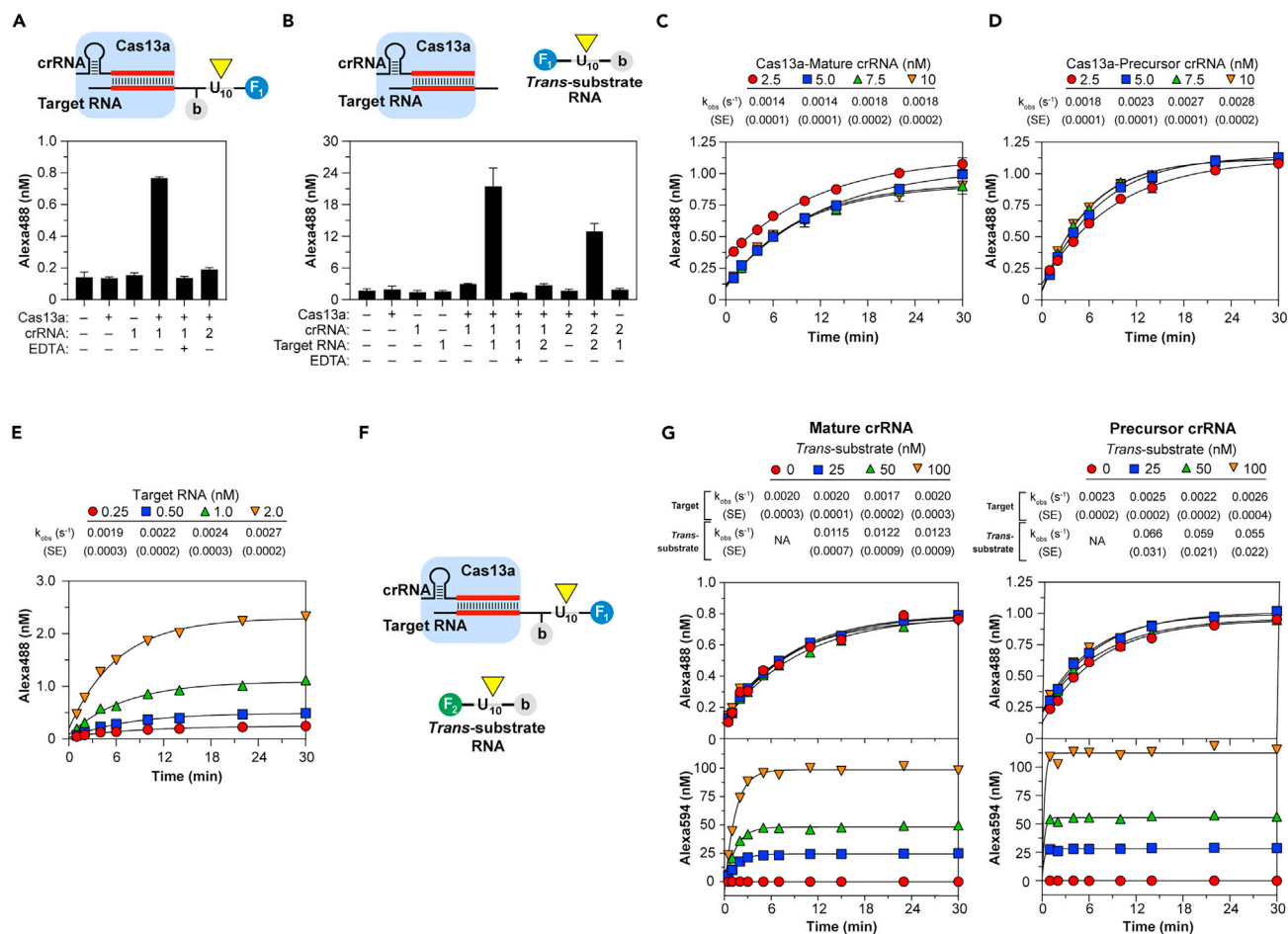


Figure 2. Cas13a cleavage of target RNA and activation of trans-RNase

(A) Cas13a cleavage (yellow triangle) of dual-labeled target. Components tested on Fluorescent Target RNA-1 containing sequence targeted by crRNA-1 but not -2. (B) Target-activated Cas13a cleavage of dual-labeled trans-RNA U_{10} . (C–E) Single-turnover target cleavage using 1.0 nM Fluorescent Target RNA-1 reacted with varied Cas13a bound to mature (C) or precursor (D) crRNA-1 or varied Fluorescent Target RNA-1 reacted with 5.0 nM Cas13a bound to precursor crRNA-1 (E). Lines show single-exponential fit to yield k_{obs} . (F–G) Simultaneously recorded target and trans cleavage: RNP reacted with a mixture of Alexa 488 (F_1)-tagged target RNA and Alexa 594 (F_2)-tagged trans-substrate. Time courses were recorded on 5.0 nM Cas13a bound to mature or precursor crRNA-1, then reacted with a mixture of 1.0 nM Alexa 488-labeled Target RNA-1 and varied Alexa 594-labeled trans-RNA U_{10} . Lines show single-exponential fit (where applicable) for target (top) or trans cleavage (bottom) to yield k_{obs} . In panels (A–C and E) data represent mean \pm standard deviation (SD). See also Figures S2 and S3.

Kinetic constants for non-target RNA trans-cleavage were determined by pre-reacting RNP with target, then measuring initial velocities (V_0) for trans-cleavage (Figure 3D). Using the mature crRNA-Target-1 activating pair, V_0 for U_5 and U_{10} increased linearly without signs of approaching saturation, indicating a $K_M > 1 \mu M$ (Figure 3E); kinetic constants estimated from direct dependence of V_0 on substrate concentration (Figure S3D; Tables S1 and S4) gave k_{cat}/K_M of $0.33 \times 10^7 M^{-1} s^{-1}$ and $1.0 \times 10^7 M^{-1} s^{-1}$ and lower limit estimates for k_{cat} of $3.3 s^{-1}$ and $12 s^{-1}$, respectively. A similar k_{cat}/K_M was obtained for U_{10} using four-fold higher RNP (Figure S3J), validating the use of target concentration as a proxy for that of activated enzyme, further indicating the K_d of target binding to RNP is $< 2.5 nM$. Saturation kinetics observed for U_{20} enabled determination for K_M of 760 nM and k_{cat} of $17 s^{-1}$ (Figure 3E), yielding a k_{cat}/K_M of $2.2 \times 10^7 M^{-1} s^{-1}$ (Table 1), corroborated by analysis at substrate concentrations below K_M (Figure S3D; Table S4). Together, these results confirm that post-binding trans-cleavage rates are considerably greater than those measured for target cleavage.

Trans-cleavage of U_{10} and U_{20} activated by a mature crRNA-target pair (crRNA-Target-3) eliciting greater trans-RNase activity showed its higher efficiency arises mainly from increased k_{cat} (Tables S1 and S4; Figures

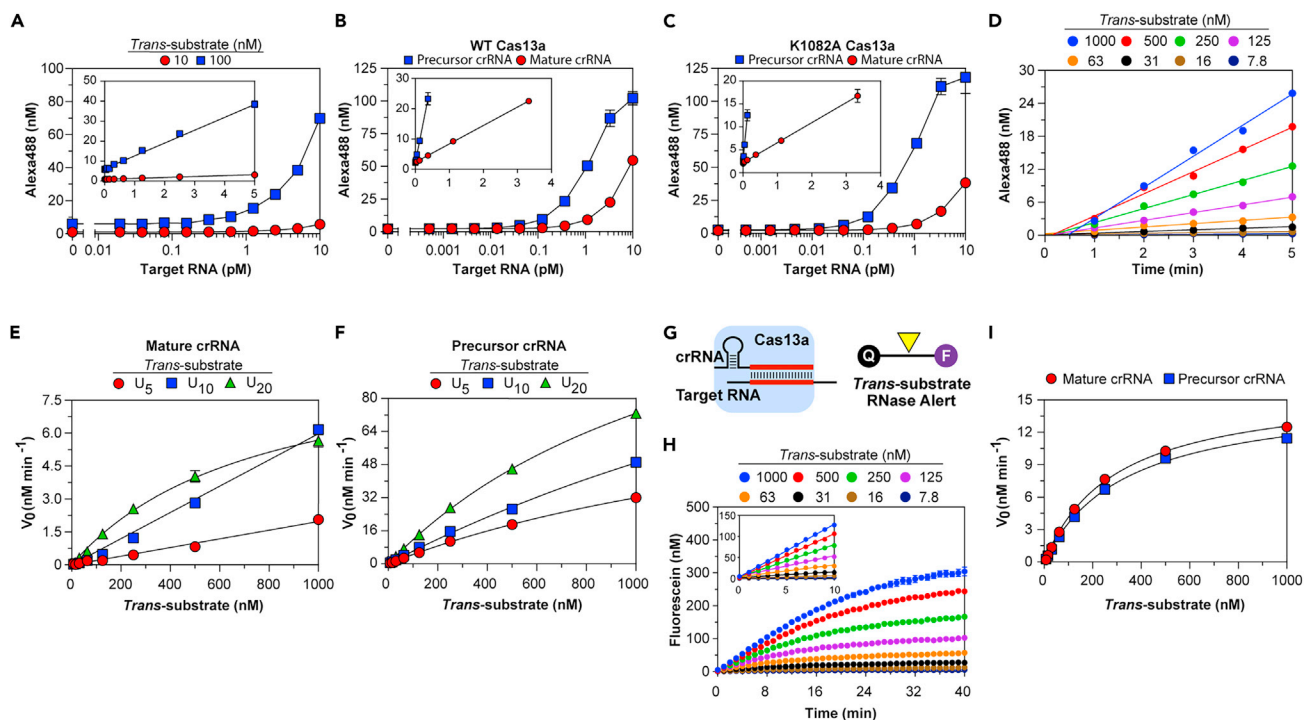


Figure 3. Characterization of target-activated Cas13a trans-RNase

(A–C) Varied Target RNA-1 and *trans*-RNA U₁₀ were reacted with WT (A, B) or processing mutant K1082A (C) Cas13a bound with mature (A) or both mature and precursor (B, C) crRNA-1. (Insets) Lines show linear fit to yield k_{app} (see Table S3). (D–F) *Trans*-cleavage using Cas13a bound with mature (D, E) or precursor (F) crRNA-1, activated with 10 pM Target-1, then reacted with varied *trans*-RNA. Lines show linear fit of time course of U₂₀ cleavage to determine V₀ (D) or V₀ dependence on substrates U₅ and U₁₀ substrates (E) or hyperbolic fit of all others (E – F) to yield kinetic constants (Table 1). (G–I) Target-activated Cas13a RNP cleaves RNaseAlert, untethering quencher (Q) from fluorescein (F). Cas13a bound to mature (H, I) or precursor (I) crRNA-1 was activated by 10 pM Target RNA-1, then reacted with substrate, and fluorescence was recorded continuously (H). Lines show linear fit to determine V₀ (H, Inset) or hyperbolic fit of V₀ dependence on substrate (I) to yield kinetic constants (Table 1). Data in panels (A–C and H) represent mean \pm SD and in (E, F, I) represent value \pm standard error (SE). See also Figures S2 and S3 and Tables S3 and S4.

S3G and S3H). Again, precursor crRNA stimulated a more active Cas13a *trans*-RNase than mature, processed forms for two different crRNA-target pairs (Figures 3E, 3F, S3D, S3E, S3G, and S3H; Tables S1 and S4). For the most active Cas13a *trans*-RNases, k_{cat} and K_M were together highest for U₁₀ (Table 1): k_{cat} values were as high as 360–740 s⁻¹. The close agreement between kinetic constants obtained from steady-state analysis and endpoint measurements (Table S3) demonstrates *trans*-activity is maintained for at least 1 hr at 37°C. As expected for a cellular RNA degraded by *trans*-RNase activity *in vitro* (East-Seletsky et al., 2016), tRNA competed for U₂₀ cleavage (Figure S3K).

Finally, *trans*-cleavage of RNaseAlert (Figures 3G–3I) exhibited saturation kinetics for all crRNA-target pairs tested and reduced k_{cat} and K_M compared to those for polyuridine substrates (Table 1). Moreover, for Cas13a activated by mature or precursor crRNA, or by different crRNA-target pairs, kinetic constants for RNaseAlert varied only slightly: K_M ranged between 101 and 330 nM, k_{cat} ranged from 17–35 s⁻¹, and k_{cat}/K_M spanned 0.78–1.1 $\times 10^8$ M⁻¹ s⁻¹ (Figures 3I and S3I; Table 1). Estimates of k_{cat}/K_M for RNaseAlert from V₀ at low substrate concentrations corroborated values obtained by Michaelis-Menten analysis (Figures S3F and S3I; Table S4). These results indicate that the use of RNaseAlert does not record the full catalytic potential of Cas13a, nor does it reflect differences in catalytic activity that may arise from the crRNA processed form or the activating crRNA-target combination.

Cas12a: target cleavage and trans-nuclease activation

To develop a Cas12a-based diagnostic, we sought to better understand steps leading to activation of its RuvC domain by performing kinetic analysis of LbCas12a crRNA-guided target and *trans*-cleavage. We

Table 1. Kinetic constants for trans-cleavage of nuclei acids by crRNA-target-activated Cas enzymes

Enzyme	crRNA (form)	Target	Trans-substrate ^a	k_{cat} (s ⁻¹)	K_M (nM)	k_{cat}/K_M (M ⁻¹ s ⁻¹)	Figure
Cas13a	1 (mature)	1	U ₅ ^b	>3.3	>1000	$3.3 (\pm 0.2) \times 10^6$	3E
			U ₁₀ ^b	>12	>1000	$1.03 (\pm 0.03) \times 10^7$	3E
			U ₂₀	16.7 (±0.9)	760 (±70)	$2.2 (\pm 0.2) \times 10^7$	3E
			RNaseAlert	27.1 (±0.6)	294 (±16)	$9.2 (\pm 0.5) \times 10^7$	3I
	1 (precursor)	1	U ₅	164 (±7)	2100 (±120)	$7.9 (\pm 0.5) \times 10^7$	3F
			U ₁₀	360 (±50)	3400 (±600)	$1.1 (\pm 0.2) \times 10^8$	3F
			U ₂₀	290 (±8)	1390 (±60)	$2.1 (\pm 0.1) \times 10^8$	3F
			RNaseAlert	25.8 (±0.7)	330 (±20)	$7.8 (\pm 0.5) \times 10^7$	3I
	3b (mature)	3	U ₁₀	320 (±10)	2230 (±90)	$1.43 (\pm 0.08) \times 10^8$	S3G
			U ₂₀	273 (±6)	1500 (±50)	$1.82 (\pm 0.07) \times 10^8$	S3G
			RNaseAlert	17.1 (±0.3)	101 (±6)	$1.7 (\pm 0.1) \times 10^8$	S3I
	3 (precursor)	3	U ₁₀	740 (±40)	3500 (±200)	$2.1 (\pm 0.2) \times 10^8$	S3H
U ₂₀			360 (±30)	1100 (±100)	$3.2 (\pm 0.4) \times 10^8$	S3H	
RNaseAlert			24.9 (±0.7)	220 (±20)	$1.1 (\pm 0.1) \times 10^8$	S3I	
Cas12a	1 (mature)	1	C ₁₀	2.77 (±0.05)	28 (±2)	$9.8 (\pm 0.7) \times 10^7$	5D
			C ₂₀	2.26 (±0.08)	28 (±4)	$8.0 (\pm 1.0) \times 10^7$	S4C
			DNaseAlert	1.30 (±0.03)	26 (±2)	$5.1 (\pm 0.4) \times 10^7$	5E
			dsDNA	0.044 (±0.001)	13 (±1)	$3.5 (\pm 0.7) \times 10^6$	5F
			U ₂₀	0.118 (±0.005)	133 (±17)	$8.9 (\pm 1.1) \times 10^5$	5G
			IS2404	C ₁₀	1.32 (±0.04)	49 (±4)	$2.7 (\pm 0.2) \times 10^7$
	2 (mature)	2	C ₁₀	3.83 (±0.18)	35 (±5)	$1.1 (\pm 0.2) \times 10^8$	5D
			C ₂₀	2.28 (±0.05)	18 (±2)	$1.3 (\pm 0.1) \times 10^8$	S4C
			DNaseAlert	1.02 (±0.03)	23 (±2)	$4.4 (\pm 0.5) \times 10^7$	5E
			dsDNA	0.054 (±0.002)	16 (±2)	$3.3 (\pm 0.4) \times 10^6$	5F
			U ₂₀	0.338 (±0.008)	108 (±8)	$3.2 (\pm 0.2) \times 10^6$	5G

^aTrans-substrate: C₁₀ and C₂₀ are ssDNA; U₅, U₁₀ and U₂₀ are ssRNA.

^bEstimates based on direct dependence of V_0 on substrate concentration through entire concentration range.

used the substrate-capture approach to measure cleavage of dsDNA targets containing a dual-labeled TS (Figure 4A) to record double-stranded cleavage, since Cas12a proceeds with NTS first, and cleavage of ssDNA trans-substrates labeled at opposite ends (Figure 4B). As expected, both target and trans-cleavage require complementarity between crRNA spacer and target and presence of divalent cations.

Target cleavage was performed under single-turnover conditions using mature crRNA-Cas12a in excess over target. At 37°C, cleavage proceeded with k_{obs} of 0.023 s⁻¹ (Figure S4A) and two-fold more slowly (k_{obs} 0.012 s⁻¹) at 25°C (Figure 4C), the temperature chosen for further studies, at a rate independent of RNP concentration above 2.5 nM. Similar cleavage rates independent of target concentration spanning 0.5 to 2.0 nM were observed (Figure 4D). Unlike Cas13a, target cleavage by precursor crRNA-Cas12a forms, containing additional 15- and 6-nt 5' to the processing site, were no different (Figure S4B). These results suggest target binds rapidly to RNP with a dissociation constant considerably <2 nM, and its cleavage is rate-limited by a post-binding step, in agreement with studies demonstrating slow unwinding of target strands and formation of an R-loop preceding cleavage of bound target DNA in AsCas12a (Strohkendl et al., 2018).

To test whether the appearance of trans-nucleolytic activity is also limited by a post-target binding step, target and trans-cleavages were monitored simultaneously by reacting RNP with mixtures of target and trans-substrate labeled with distinguishable Alexa tags (Figure 4E). Target cleavage rates were similar to those measured above and were not affected by the presence of trans-substrates, and trans-cleavage exhibited a lag phase of a similar duration as target cleavage (k_{obs} 0.011–0.024 s⁻¹). After this lag, trans-

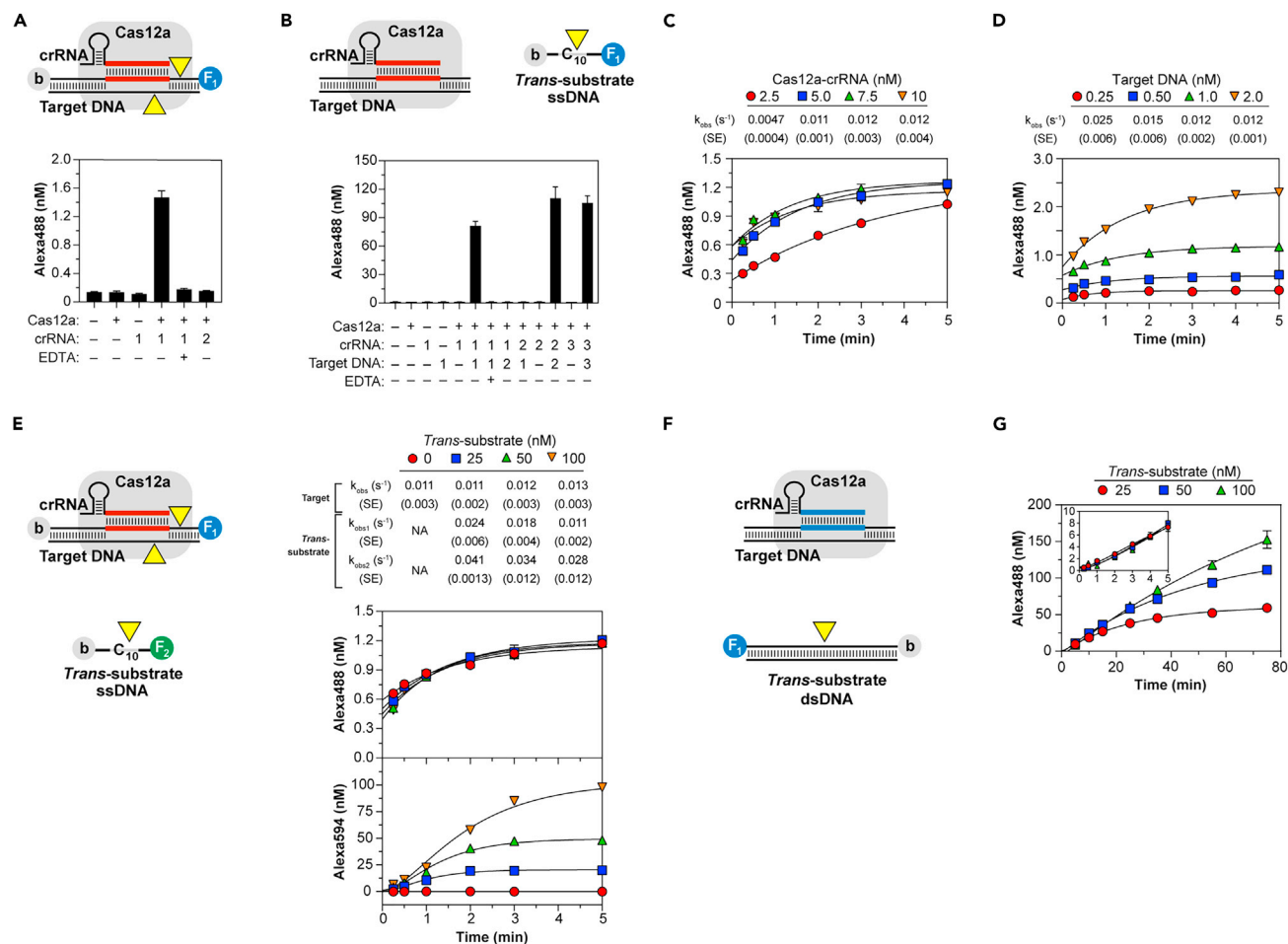


Figure 4. Cas12a cleavage of target DNA and activation of trans-nuclease

(A) Cas12a cleavage of dual-labeled target dsDNA. Components tested on Fluorescent Target DNA-1 containing protospacer specified by crRNA-1 but not -2. (B) Target-activated Cas12a cleavage of dual-labeled *trans*-ssDNA. Components tested on substrate C₁₀. (C and D) Single-turnover target cleavage using varied Cas12a-crRNA-1 reacted with 1.0 nM Fluorescent Target DNA-1 (C) or 5.0 nM Cas12a-crRNA-1 reacted with varied Fluorescent Target DNA-1 (D). Lines show single-exponential fit to yield k_{obs} . (E) Simultaneously recorded single-turnover target and multiple-turnover *trans*-cleavage using dual-labeled dsDNA target tagged with Alexa 488 (F₁) and *trans*-ssDNA tagged with Alexa 594 (F₂). 5.0 nM Cas12a-crRNA-1 was reacted with a mixture containing 1.0 nM Alexa 488-labeled Target DNA-1 and varied Alexa 594-labeled C₁₀. Lines show single-exponential (target cleavage, top) or sequential double-exponential (*trans*-cleavage, bottom) fit to yield k_{obs} . (F) Multiple-turnover cleavage of dual-labeled non-target *trans*-dsDNA. 5.0 nM Cas12a-crRNA-2 was reacted with mixtures containing 1.0 nM unlabeled Target DNA-2 and varied Fluorescent Target DNA-1 at 37°C. Lines show sequential double-exponential fit to yield a lag phase followed by accumulation of product (k_{obs} 0.017–0.018 s⁻¹). (Inset) Similar experiment of shorter duration. In all panels data represent mean ± SD. See also Figures S4 and S5.

cleavage accelerated during the steady-state phases as the substrate was increased from 25 to 100 nM, indicating *trans*-ssDNA cleavage operates below its maximal velocity under these conditions. Together, these results indicate activation of Cas12a *trans*-activity is also rate-limited by post-target binding steps, suggesting its initiation is coupled to target cleavage.

Target-activated dsDNA *trans*-cleavage (see below) was then recorded by reacting RNP with mixtures of unlabeled target and dual-labeled *trans*-dsDNA lacking the crRNA-specified protospacer (Figure 4F). Because dsDNA *trans*-cleavage was considerably slower than ssDNA *trans*-cleavage, the reaction temperature was raised to 37°C to shorten the time course. Products of dsDNA *trans*-cleavage also accumulated after a lag likely reflecting rate-limiting target cleavage. However, for the first minutes after this lag, initial cleavage rates were indistinguishable over substrate concentrations of 25–100 nM (Figure 4F, inset), indicating dsDNA *trans*-cleavage operates at low, albeit maximal, and velocity under these conditions. These results indicate both ss and dsDNA *trans*-cleavage are kinetically coupled to steps involved in target cleavage.

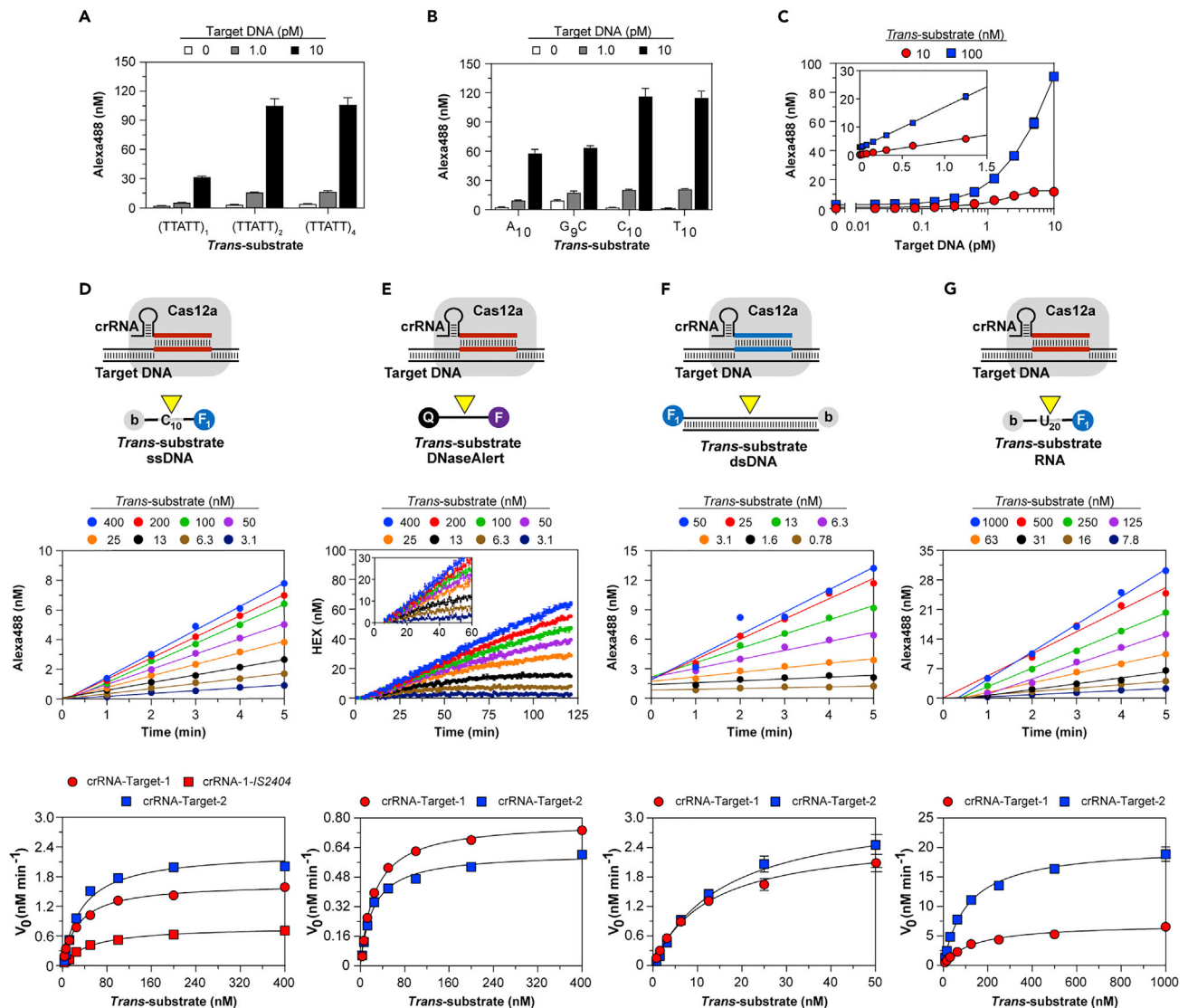


Figure 5. Characterization of target activated Cas12a trans-nuclease

(A–C) Cas12a, crRNA-1, and varied Target DNA-1 tested with trans-substrates consisting of (A) single or multiple repeats of TTATT, (B) differing sequence, or (C) varied concentrations of trans-substrate C₁₀ where linear fit was used to estimate kinetic constants (Inset). Data are represented as mean ± SD. (D–G) (Top) Cas12a RNP was pre-reacted with target, then reacted with varied trans-substrate used in each panel. (Middle) Linear fit of time courses to determine V₀. Examples shown: (D) Cas12a-crRNA-1, 10 pM Target DNA-1, substrate C₁₀; (E) Cas12a-crRNA-2, 10 pM Target DNA-2, DNaseAlert substrate; (F) Cas12a-crRNA-2, 1.0 nM Target DNA-2, non-target dsDNA substrate (Fluorescent Target DNA-1); (G) Cas12a-crRNA-1, 1.0 nM Target DNA-1, RNA substrate U₂₀. (Bottom) Hyperbolic fit of V₀ (symbols) to yield kinetic constants (Table 1); data are represented as value ± SE. See also Figures S4 and S5.

Cas12a: trans-nuclease activities

We measured trans-cleavage rates of substrates varying in length and composition. At least three-fold greater activity was observed against 10- or 20-nt substrates compared to 5-nt substrates (Figure 5A), and 10-nt ssDNA pyrimidines were at most two-fold more efficiently cleaved than those composed of purines (Figure 5B). Likewise, trans-DNase activity of *Acidaminococcus* sp. BV3L6 Cas12a (AsCas12a) showed little or no base preference (Figure S5A). Trans-activity arising from varying C₁₀ and target concentrations (Figure 5C), corresponded to k_{app} of 0.64 s⁻¹ and 2.01 s⁻¹ for 10 and 100 nM substrate, respectively, suggesting a K_M of 31 nM, k_{cat} of 2.6 s⁻¹, and k_{cat}/K_M of 8.4 × 10⁷ M⁻¹ s⁻¹. Again, RNP assembled from either mature or precursor crRNA displayed indistinguishable trans-cleavage (Figure S5B).

Though the Cas12a RuvC *trans*-nuclease has been widely described as a ssDNase, Cas12a has been reported to also cleave dsDNA and ssRNA in *trans* (Chen et al., 2017; Fu et al., 2019; Fuchs et al., 2019; Li et al., 2018; Murugan et al., 2020). We observed multi-turnover, divalent cation-dependent *trans*-cleavage of other nucleic acid substrates, including DNaseAlert (Figure S5C), widely used to monitor ssDNase *trans*-activity, non-target dsDNA (Figure S5D), and ribonucleotide U₂₀ (Figure S5E), demonstrating the substrate nucleobase indifference of the Cas12a RuvC nuclease.

To gain insight into the mechanism of *trans*-cleavage and the potential physiological relevance of the different substrates, we measured steady-state rates of *trans*-cleavage. Kinetic constants were determined by pre-reacting RNP with target, then measuring V₀ of *trans*-cleavage (Figures 5D–5G). Cas12a activated by two different crRNA-target pairs cleaved both C₁₀ and C₂₀ with kinetic constants varying only little: k_{cat} of 2.3–2.8 s⁻¹, K_M of 18–35 nM, and k_{cat}/K_M of 0.8–1.3 × 10⁸ M⁻¹ s⁻¹ (Figures 5D and S4C; Table 1). Similar constants were obtained for IS2404, a 1299-bp fragment of DNA from the pathogenic bacterium *M. ulcerans* containing protospacers specified by crRNA-1, -2, and -3. Since these values are comparable to those estimated from 2 hr endpoints (Figure 5C), *trans*-activity persists over several hours at 37°C. Furthermore, these K_M values account for the observed post-lag acceleration of *trans*-cleavage (Figure 4E). Kinetic constants remained largely unchanged when RNP concentration was increased four-fold (Figure S4D), further indicating K_d is < 2 nM and target concentration can serve as a proxy for that of activated enzymes. Kinetic constants for cleavage of polycytidine were comparable to those for DNaseAlert determined via a parallel approach for both crRNA-target pairs (Figures 5E and S4E; Table 1). Increasing ionic strength with additional salt or including the heparin polyanion decreased cleavage efficiency of both C₁₀ and DNaseAlert by increasing K_M with minimal effect on k_{cat} (Figures S4F and S4G). Together, these results demonstrate steady-state *trans*-cleavage of ssDNA and DNaseAlert (k_{cat} 1–3 s⁻¹) is considerably faster than the rate-limiting step in target cleavage.

Multi-turnover *trans*-cleavage of dsDNA by Cas12a (Figure 5F) activated by two crRNA-target pairs was considerably less efficient than ssDNA, with k_{cat}/K_M of 3.3–3.5 × 10⁶ M⁻¹ s⁻¹, primarily due to 60–70-fold reduction of k_{cat} to 0.04–0.05 s⁻¹ and reduction of K_M to 13–16 nM (Table 1). Besides illustrating the strong structural preference for single-stranded *trans*-substrates, these results account for the approach of Cas12a to a low, albeit maximal, velocity for *trans*-dsDNA cleavage (Figure 4F). Finally, k_{cat} for multi-turnover ssRNA *trans*-cleavage (Figure 5G) by Cas12a activated by both crRNA-target pairs was only 1/10th that for ssDNA and, combined with higher K_M, resulted in considerably lower catalytic efficiencies, with k_{cat}/K_M of 0.9–3.2 × 10⁶ M⁻¹ s⁻¹ (Table 1). Thus, steady-state analysis indicates *trans*-nucleolytic activity of the Cas12a RuvC domain may be described as a preferential DNase structurally selective for single-stranded substrates.

Cas13a and Cas12a: quantitative, amplification-free Detection of Pathogen Nucleic Acids

To illustrate their utility, we applied the findings to improve assay sensitivity to enable amplification-free detection of nucleic acid targets. Having shown that the RNP-target affinity was sufficiently high—K_d is considerably less than typical assay RNP concentrations—we predicted multiple protospacers could be bound by RNP assembled from pools of multiple crRNA species, generating *trans*-cleavage activity greater than that of single target-RNP. We screened 21 Cas13a crRNA-target pairs corresponding to different regions of hepatitis C viral RNA, assessing apparent turnover rates from endpoint values (Figure 6A). Of these, we identified 13 non-overlapping crRNA, which, when pooled, increased the apparent *trans*-cleavage rate 10-fold and enhanced the sensitivity for detection of pooled RNA targets by a factor of 6- to 7-fold using U₂₀ or RNaseAlert *trans*-substrates (Figure 6B; Table S5). We estimate if such targets were encoded within intact viral genomes, then the analytical limit of detection (LOD) by the pooled crRNA, 29 fM (based on 13 pooled targets), would translate to 2 fM of viral genomes.

We then developed a sensitive Cas12a-based assay to detect *M. ulcerans*, the causative agent of Buruli ulcer disease (Johnson et al., 2005), which harbors multiple copies of IS2404. Cas12a *trans*-cleavage was activated by DNA isolated from *M. ulcerans*, but not from the related bacterium *M. tuberculosis*, which lacks IS2404, or from *E. coli* or humans as they do not have a crRNA-complementary protospacer and an adjacent PAM (Figures 6C and 6D). We screened 39 crRNA designed to target protospacers adjacent to PAM sequences within IS2404 for *trans*-nuclease activity (Figure 6E). Perhaps worth further study, higher activity was observed for several crRNA guiding Cas12a to protospacers within 5' AND-3' untranslated regions of the IS2404 transposase gene (Figure S6A). Four sub-pools from the 20 highest potency crRNA, excluding those demonstrating pairwise interference (Figures S6B–S6D), cumulatively increased *trans*-activity of Cas12a (Figure 6F). The use of 20-pooled crRNA increased k_{app} and enhanced detection of IS2404, for

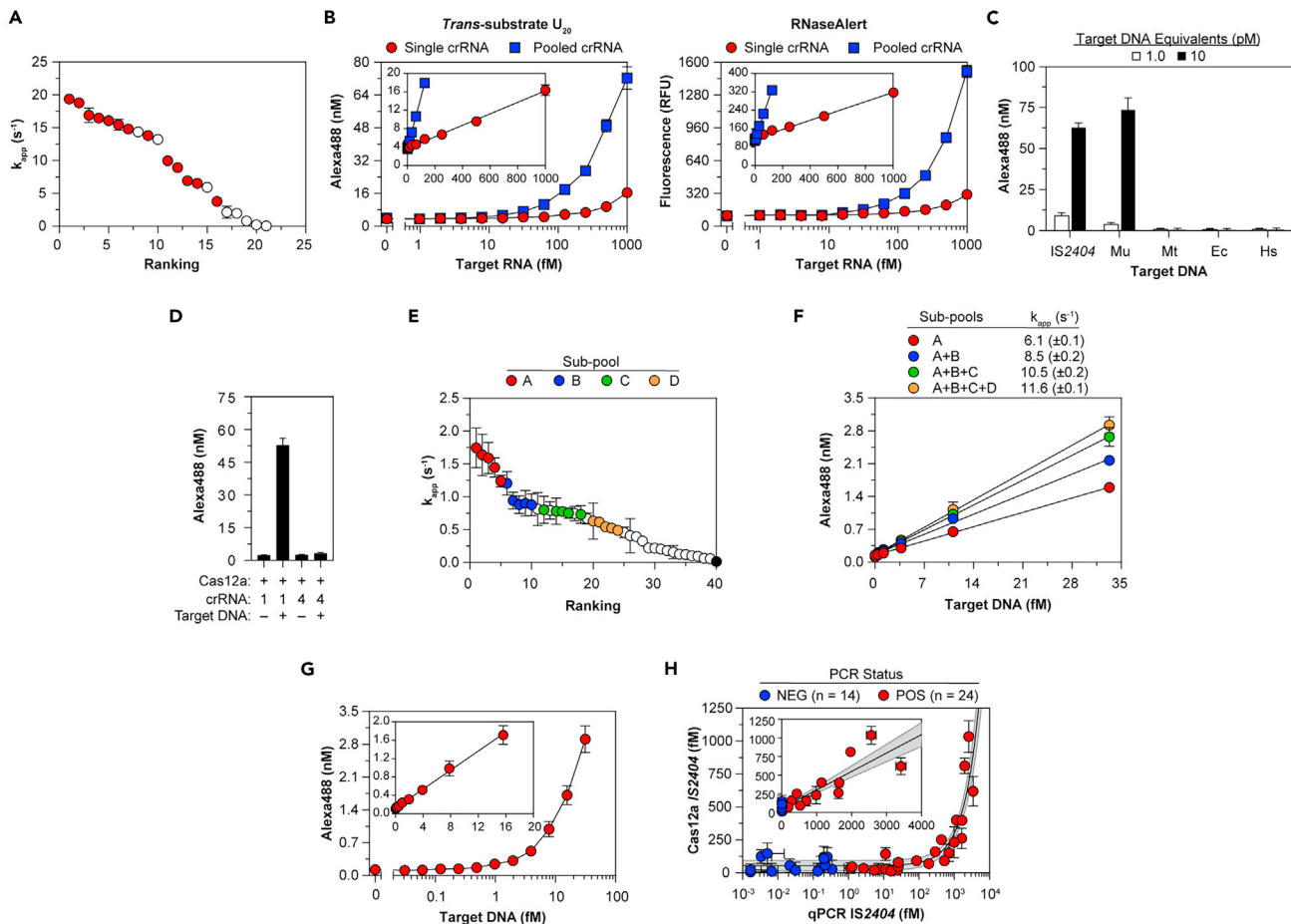


Figure 6. Pooling of crRNA enables sensitive cas-directed detection of pathogen nucleic acids

(A) *Trans*-RNase activity of Cas13a bound to individual precursor crRNA, then reacted with target RNA and *trans*-RNA U_{10} . Filled symbols indicate 13 crRNA selected for pooling. (B) *Trans*-RNase activity of Cas13a bound to single or 13 pooled crRNA, then reacted with 13 pooled target RNA and U_{20} (left) or RNaseAlert (right). (Insets) Linear fit to yield k_{app} (Table S5). (C) *Trans*-DNase activity of Cas12a bound to crRNA-1, then reacted with IS2404 or genomic DNA and *trans*-ssDNA C_{10} . Genomic DNA isolated from *M. ulcerans* (Mu) contains IS2404 protospacers targeted by crRNA-1, whereas genomic DNA isolated from *M. tuberculosis* (Mt), *E. coli* (Ec), and humans (Hs) do not. (D) *Trans*-DNase activity of components tested on C_{10} . Protospacer in target IS2404 complementary to crRNA-1 abuts a PAM, whereas that of crRNA-4 does not. (E) *Trans*-DNase activity of Cas12a bound to individual crRNA, then reacted with IS2404, which contains protospacers for each crRNA, and C_{10} . Colors indicate 20 crRNA selected for sub-pooling. Activity of Cas12a-crRNA-4 is indicated by black symbol. (F–G) *Trans*-DNase activity of Cas12a bound to crRNA pools added cumulatively (F) or together (G), then reacted with IS2404 and C_{10} . Linear fits were used to calculate k_{app} (see Table S5). (H) IS2404 in DNA samples isolated from 38 patient skin swabs quantified by Cas12a *trans*-activity (y axis) or by qPCR (x axis). Color-coded patient qPCR status was determined from DNA extracted initially at test site. Solid line, detailed in Inset, indicates linear fit to yield k_{app} (Table S5); gray shading indicates 95% confidence interval. In all panels data represent mean \pm SD. See also Figure S6 and Table S5.

which an analytical LOD of 310 aM was determined (Figure 6G; Table S5). By calibrating the *trans*-activity of Cas12a loaded with the 20-pooled crRNA against IS2404, we quantified the concentration of IS2404 in DNA extracted from wound swabs of 38 patients suspected to be infected with *M. ulcerans*, whose disease status was originally ascertained using IS2404 qPCR at the field hospital where samples were collected (Figure 6H). Linear analysis indicated Cas12a detects ~25% of qPCR-identified IS2404 segments in DNA isolates. Thus, sensitive and quantitative detection of nucleic acid targets by Cas enzymes may be achieved by combining multiple crRNA.

DISCUSSION

Cas13a: target RNA cleavage and *trans*-nuclease activation

Target RNA binding to Cas13a RNP is rapid, achieving equilibrium within seconds, and does not limit its cleavage rate. We estimate the K_d for initial encounter complex formation is < 1 nM, approximately 20-fold lower than

measured for LbuCas13a in the presence of tRNA (Tambe et al., 2018), a potential competitive inhibitor that decreases *trans*-cleavage efficiency by approximately 100-fold. We observed Cas13a target cleavage to be considerably slower than steady-state *trans*-cleavage, indicating constraints in this particular target or some other post-binding step limit its cleavage. It remains unknown whether target cleavage proceeds in *cis* via *intra*-molecular cleavage by the same Cas13a to which it is bound or in *trans* via *inter*-molecular cleavage by a separate activated Cas13a RNP, as in the LbuCas13a dimeric complex (Liu et al., 2017). Though 5'-extended targets may not readily access the RNase site, longer targets might be more efficiently cleaved in *cis* if not physically constrained. *Trans*-cleavage commences seconds after enzyme encounters target, indicating HEPN nuclease activation is rapid. *Trans*-cleavage rates were approximately five to ten times faster than target cleavage using Cas13a bound to either mature and precursor crRNA, indicating that activation of HEPN *trans*-nuclease activity does not generally require target cleavage nor does cleavage of targets in *cis* pose a rate-limiting barrier to *trans*-activity. Target cleavage rates remained unchanged in the presence of up to 100 nM *trans*-ssRNA, conditions whereby Cas13a can undergo multiple rounds of *trans*-cleavage, indicating *trans*-substrates may only weakly competitively inhibit target cleavage due to their high K_M values.

Our steady-state analysis of Cas13a *trans*-cleavage revealed several features of the activated catalytic state of the HEPN nuclease. First, catalytic efficiencies triggered by different crRNA-target pairs varied over a 15–30-fold range, mainly due to variations in k_{cat} , indicating different conformational states are sampled by Cas13a depending on crRNA-target duplex sequence. Notably, this variability was not observed for *trans*-cleavage of RNaseAlert, suggesting it probes a subset of the conformational states. Second, addition of nucleotides 5' to the protospacer had little or no effect on HEPN *trans*-nuclease activity. Third, precursor crRNA possessing additional nucleotides 5' to its processing site stimulate 2- to 10-fold higher catalytic efficiency than mature forms on polyuridine *trans*-substrates (but not RNaseAlert) for both the wild-type and crRNA-processing deficient variant of Cas13a. These increases were associated with increased k_{cat} . Fourth, the agreement between kinetic constants from endpoint and steady-state readings indicates the activated conformational state is maintained at high levels for at least 1 hr at 37°C. Together, these results suggest the determinants for allosteric activation of the Cas13a HEPN nuclease extend beyond the complex specificity landscape demonstrated for base pairs involved in target binding (Tambe et al., 2018).

Though variable, estimates for the HEPN *trans*-nuclease catalytic efficiency converge on a value of $\sim 10^8$ $M^{-1} s^{-1}$, providing a lower-limit bimolecular rate constant for *trans*-substrate binding to the activated enzyme, a value within two orders of magnitude of the diffusion-controlled limit. In the most highly activated forms of Cas13a, k_{cat} of several hundred per sec were observed, which is very high compared to the *trans*-nuclease activity observed for Cas12a, but within the range for other ribonucleases, including pancreatic ribonucleases in the RNase A family (EC 4.1.1.18): k_{cat} of 323 s^{-1} for bovine (Moussaoui et al., 2007) and 2317 s^{-1} for human (Rehman et al., 2011) enzymes. For Cas13a, k_{cat} for polyuridine *trans*-substrates was as much as 30 times higher than for RNaseAlert, indicating once bound, the former are more rapidly cleaved and released than the latter, and the use of RNaseAlert does not accurately record the full catalytic potential of Cas13a and may be suboptimal for diagnostics.

Spacer regions of type VI systems show complementarity to DNA, but not RNA viruses (Smargon et al., 2017; Yan et al., 2018), suggesting Cas13a is activated by viral transcripts made during infection and targets destruction of nascent transcripts (Hampton et al., 2020; Varble and Marraffini, 2019). This hypothesis is strongly supported by *in vivo* experiments demonstrating Cas13a-mediated transcript destruction suffices to disrupt phage infection (Koonin and Zhang, 2017; Meeske et al., 2019). Our observation that *trans*-RNase activity is triggered immediately and proceeds rapidly likely reflects the requirement for this mode of interference to outcompete the rapid viral transcription. The slow rate of target cleavage exposes the relatively long half-life of the ternary complex, which prevents translation of the transcript to which the enzyme is bound and enables the enzyme to undergo multiple rounds of *trans*-cleavage before releasing the target sequence, presumably deactivating nuclease activity. Further experiments are needed to determine the effect, if any, of Cas13a *trans*-RNase activity when expressed in eukaryotic cells.

Cas12a: target DNA cleavage and *trans*-nuclease activation

Our results indicate dsDNA target binding to LbCas12a RNP is rapid, likely equilibrating within seconds, and are consistent with the bimolecular constant measured for AsCas12a binding to target (Strohkendl et al., 2018). Binding is tight, with a K_d of <5 nM for initial encounter complex formation, in agreement with the values for AsCas12a (Strohkendl et al., 2018) and LbCas12a (Jeon et al., 2018). Despite rapid

binding, target cleavage is slow, consistent with previous measurements with Lb and AsCas12a (Jeon et al., 2018; Knott et al., 2019; Strohkendl et al., 2018). Given the steady-state rate of ssDNA *trans*-cleavage is almost 100-fold faster, our results agree with a model whereby NTS and TS are rapidly cleaved following slow rate-limiting strand unwinding and R-loop formation (Stella et al., 2018; Strohkendl et al., 2018).

Our results show *trans*-nuclease activity proceeds via two kinetically resolvable steps. The first appears as a lag in *trans*-cleaved product accumulation at a rate corresponding to target cleavage, comparable to TS cleavage rates and PAM-distal target fragments release measured for AsCas12a (Strohkendl et al., 2018), indicating they likely represent the same steps in orthogonal enzymes. The second step represents *trans*-substrate binding and cleavage itself, which is considerably faster for ssDNA *trans*-substrates than for dsDNA. We conclude that *trans*-nuclease activity acquisition accompanies late steps of target DNA destruction, including TS cleavage and, perhaps, PAM-distal fragment release. Cas12a remains tightly bound to the PAM-proximal target fragment (Singh et al., 2018), locked into a conformational state capable of engaging in multiple rounds of *trans*-cleavage for 2 hr or longer at 37°C.

Cas12a *trans*-cleavage can be described in terms of a Michaelis-Menten enzyme, in agreement with previous reports (Chen et al., 2017; Knott et al., 2019). Kinetic constants for Cas12a *trans*-cleavage activated by two different crRNA-target combinations are similar, suggesting they represent general kinetic features for LbCas12a activated by fully matched pairs. The LbCas12a k_{cat} of $\sim 2 \text{ s}^{-1}$ for polycytidine *trans*-substrates is similar to the NTS cleavage rate ($>4 \text{ s}^{-1}$) of the Cas9 RuvC domain (Gong et al., 2018) but is smaller than rates exhibited by other DNases, such as the single-strand-specific, non-sequence-specific endonuclease S1 (k_{cat} of 42 s^{-1}) (Li et al., 2000) or the Cas13a *trans*-RNase (see above). Nevertheless, the low-turnover Cas12a *trans*-activity may be of physiological importance considering the double-strand-, site-specific endonuclease EcoRI, a component of the bacterial modification system providing defense against invading viruses, cleaves targets with k_{cat} of 0.063 s^{-1} (Modrich and Zabel, 1976). The k_{cat}/K_M ratio of $\sim 10^8 \text{ M}^{-1} \text{ s}^{-1}$ for Cas12a *trans*-cleavage represents a bimolecular rate constant lower limit estimate for *trans*-substrate binding to the enzyme ternary complex, suggesting target DNA binding and cleavage serve as the main allosteric switch activating *trans*-nuclease activity. Finally, we show kinetic properties for *trans*-cleavage of DNaseAlert are like those for polycytidine substrates, demonstrating that its cleavage can serve as a generalized marker for activation of the Cas12a *trans*-nuclease.

We interpret *trans*-cleavage activities of Cas12a against different substrates in context of a proposed two- Mg^{2+} mechanism, whereby catalytic residues and the scissile phosphate jointly coordinate metal ions roughly in line with the phosphoribosyl backbone on opposite sides of target bases (Yang et al., 2006). Lack of *trans*-nucleobase preference by both Lb and AsCas12a suggests most contacts between enzyme and substrate, as well as DNA target (Swarts et al., 2017), are mediated through the phosphoribosyl backbone. Inhibition of *trans*-cleavage by polyanionic heparin suggests non-specific electrostatic interactions help steer *trans*-substrates into the catalytic site. Preference for *trans*-substrates containing deoxyribose suggests the RNA 2' OH interferes with the positioning of the metal ions. LbCas12a prefers single-stranded *trans*-substrates, even though the attack of the phosphoribosyl backbone by RuvC nucleases does not require gross distortion of the phosphate backbone or base unstacking (Yang, 2011), similar to the structural preference displayed by other RuvC domains characterized to date, including Cas9, as well as the bacterial Holliday junction-resolving endonuclease RuvC itself (Górecka et al., 2019). Low-level Cas12a *trans*-activity against dsDNA likely represents cleavage of denatured single-stranded ends of duplexes and may represent the same low-level nicking of dsDNA observed by others (Murugan et al., 2020) on localized regions of dynamically melted DNA strands providing transient access for cleavage. Structural selectivity for single-strands and base indifference are likely to be general properties of the Cas12a RuvC nuclease, reflecting both that dsDNA target cleavage requires R-loop formation and specificity for target cleavage is governed not by the catalytic site itself but rather by sequences involved in crRNA-target hybridization, enabling Cas12a to act as a generic nuclease against any number of invading protospacers.

Experimental data probing the physiological role of Cas12a, including *trans*-nuclease activity, is currently lacking, though both nuclease activities play essential roles in interference with target cleavage degrading infectious dsDNA, similar to most CRISPR systems including Cas9, and *trans*-activity targeting ssDNA species in transcription bubbles or during rolling circle replication (Hampton et al., 2020; Varble and Marraffini, 2019). *Trans*-nuclease activity of ssDNA is conserved among members of type V systems (Yan et al., 2019) and is also key to type III systems, supporting this hypothesis. Our observation that target cleavage is a

prerequisite for *trans*-nuclease activation may reflect the relative importance of the two viral interference activities. Based on the relatively low efficiencies for cleavage of dsDNA and RNA in *trans*, we hypothesize these activities are of little physiological significance. While Cas12a *trans*-ssDNase activity appears to have no consequences in the context of genome editing (Wei et al., 2021), similar non-specific ssDNA cleaving Cas enzymes were recently shown to drive host mutations (Mo et al., 2021).

Cas13a and Cas12a: quantification of pathogen nucleic acids in clinical specimens

We show that for both Cas13a and Cas12a, different crRNA generate widely varying *trans*-activities. From kinetic analysis, we improved sensitivity of Cas13a for target RNA by replacing mature crRNA with precursor forms activating higher *trans*-activity. Further, we capitalized on the high affinities of RNP for targets to develop a crRNA pooling strategy that enables targeting of up to twenty sequences to improve the sensitivity of both Cas enzymes. This strategy drives the analytical LOD for Cas13a down to the low femtomolar range (for viral genome equivalents) and Cas12a to the attomolar range. Moreover, we could quantifiably detect pathogen DNA in clinical specimens from patients experiencing Buruli ulcer disease—a devastating, neglected tropical disease that often goes undetected due to the lack of diagnostics appropriate for low-resource settings (Siegmund et al., 2007; Yotsu et al., 2018). Further experiments are needed to ascertain how well Cas12a-based detection of IS2404 correlates with clinical features and outcomes and what role it may play as a diagnostic.

The COVID-19 pandemic highlighted the importance of having multiple diagnostic options for disease management, especially during outbreaks. Point-of-care solutions, including antigen tests (LOD ~200 aM), are often more appropriate than highly sensitive RT-qPCR (LOD ~2 aM) (Larremore et al., 2020). Already a large number of reports have demonstrated detection of SARS-CoV-2 using Cas enzymes. In most cases NAATs were used to pre-amplify target sequences, and it is difficult to imagine how these chemistries could be used at the point-of-care without employing costly closed assay architectures to limit cross-contamination. Our approach of tuning assay conditions to optimally exploit the kinetic properties of Cas enzymes drops the LOD of non-NAAT amplified reactions to be compatible with SARS-CoV-2 nasopharyngeal samples (20 aM–20 fM), among other diseases (Nouri et al., 2021). While our paper was under review, a similar strategy was used to detect SARS-CoV-2 RNA in extracted patient samples (Fozouni et al., 2021). Synergizing with recent advances in Cas-based diagnostics for low-resource settings, including lyophilization to avoid cold chain requirements (Curti et al., 2021; Lee et al., 2020), this new class of diagnostics may meet the World Health Organization's ASSURED criteria of being affordable, sensitive, specific, user-friendly, robust, equipment-free, and deliverable to end-users.

Conclusions

We developed a quantitative experimental approach to uncover key kinetic details of the steps in activation of nucleolytic activities and potential physiological roles of representative type V and VI Cas enzymes. This approach may be used to investigate the catalytic properties of other Cas enzymes, as well as other nucleases. Further, we applied these findings to design a novel approach for quantitative diagnostic applications using Cas enzymes and anticipate these findings may also guide engineering of Cas enzymes for gene editing.

LIMITATIONS OF THE STUDY

Given the wide range of *trans*-cleavage activities displayed by different Cas-crRNA RNP on a given target (Figures 6A and 6E), we anticipate that kinetic constants, which we have determined for representative Cas enzyme-crRNA-target combinations (Tables S1, S3, and S4), will likewise vary considerably. Though we have shown that analytical sensitivity for both Cas12a- and Cas13a-based assays is increased by crRNA pooling (Figure 6, Table S5), we have not tested whether signals are generated in both assays from different but related pathogen nucleic acids. As expected, individual Cas-crRNA RNP are specific for their intended targets (see Figures 2A and 2B for Cas13a and Figures 4A, 4B, 6C, S5D, and S5E for Cas12a), and we do not anticipate that crRNA pooling will have any effect on specificity.

STAR★METHODS

Detailed methods are provided in the online version of this paper and include the following:

- KEY RESOURCES TABLE

- **RESOURCE AVAILABILITY**
 - Lead contact
 - Material availability
 - Data and code availability
- **EXPERIMENTAL MODELS AND SUBJECT DETAILS**
 - Patient samples
- **METHOD DETAILS**
 - Enzymes, RNA, and DNA
 - Substrate-capture and product quantification
 - Cas13a nuclease assays
 - Cas12a nuclease assays
 - Fluorophore quantification and data analysis
 - Nuclease digestion of nucleic acid reporter probes
 - Creation of crRNA pools
 - Analysis of patient samples
- **QUANTIFICATION AND STATISTICAL ANALYSIS**

SUPPLEMENTAL INFORMATION

Supplemental information can be found online at <https://doi.org/10.1016/j.isci.2021.102996>.

ACKNOWLEDGMENTS

The authors thank Brittney Thornton for technical assistance and Ted Baughman, Joshua Bishop, Shannon Kuyper, Akos Somoskovi, David Bell, and Robert Jenison for valuable discussions. E.A.N., N.P., P.J.Y.L., Z.I., R.M.K., I.P., A.-L.M.L.N., and D.M. were supported by the Intellectual Ventures Global Good Fund. J.A.D. was supported by NIH grant nos. RM1HG009490 and U01AI142817-02, the William M. Keck Foundation, the National Multiple Sclerosis Society, NSF grant no. 1817593, the Paul Allen Frontiers Group, and the Howard Hughes Medical Institute. G.J.K. was supported by an NHMRC Investigator Grant (EL1, 1175568) and previously by an American Australian Association Fellowship. E.M. was supported by the Raoul Follereau Fondation.

AUTHOR CONTRIBUTIONS

Conceptualization, E.A.N., A.-L.M.L.N., and D.M.; Methodology, E.A.N., A.-L.M.L.N., and D.M.; Investigation, E.A.N., N.P., P.J.Y.L., Z.I., R.M.K., and I.P.; Resources, E.M., G.J.K., and J.A.D.; Writing- Original Draft, E.A.N.; Writing – Review and Editing, A.-L.M.L.N., D.M, G.J.K., and J.A.D.

DECLARATION OF INTERESTS

Some methods described herein have patents pending on which E.A.N., P.J.Y.L., G.J.N., J.A.D, A.-L.M.L.N, and D.M are inventors. The Regents of the University of California have patents issued and pending for CRISPR technologies on which G.J.K. and J.A.D. are inventors. J.A.D. is a cofounder of Caribou Biosciences, Editas Medicine, Scribe Therapeutics, and Mammoth Biosciences; is a scientific advisory board member of Caribou Biosciences, Intellia Therapeutics, eFFECTOR Therapeutics, Scribe Therapeutics, Mammoth Biosciences, Synthego, and Inari; is a director at Johnson & Johnson; and has research projects sponsored by Biogen and Pfizer.

Received: September 8, 2020

Revised: July 14, 2021

Accepted: August 13, 2021

Published: September 24, 2021

REFERENCES

- Abudayyeh, O.O., Gootenberg, J.S., Konermann, S., Joung, J., Slaymaker, I.M., Cox, D.B., Shmakov, S., Makarova, K.S., Semenova, E., Minakhin, L., et al. (2015). C2c2 is a single-component programmable RNA-guided RNA-targeting CRISPR effector. *Science* 353, 1–23.
- Aslanzadeh, J. (2004). Preventing PCR amplification carryover contamination in a clinical laboratory. *Ann Clin Lab Sci* 34, 389–396.
- Bissonnette, L., and Bergeron, M. (2006). Next revolution in the molecular theranostics of infectious diseases: microfabricated systems for personalized medicine. *Expert Rev Mol Diagn* 6, 433–450.
- Borst, A., Box, A.T.A., and Fluit, A.C. (2004). False-positive results and contamination in nucleic acid amplification assays: suggestions for a prevent

- and destroy strategy. *Eur J Clin Microbiol Infect Dis* 4, 289–299.
- Chen, J.S., Ma, E., Harrington, L.B., Tian, X., and Doudna, J.A. (2017). CRISPR-Cas12a target binding unleashes single-stranded DNase activity. *Science* 360, 436–439.
- Cofsky, J.C., Karandur, D., Huang, C.J., Witte, I.P., Kuriyan, J., and Doudna, J.A. (2020). CRISPR-Cas12a exploits R-loop asymmetry to form double strand breaks. *eLife* 9, e55143. <https://doi.org/10.7554/eLife.55143>.
- Curti, L.A., Primost, I., Valla, S., Alegre, D.I., Perglione, C.O., Repizo, G.D., Lara, J., Parcerisa, I., Palacios, A., Llases, M.E., et al. (2021). Evaluation of a lyophilized CRISPR-cas12 assay for a sensitive, specific, and rapid detection of SARS-CoV-2. *Viruses* 13, 420.
- East-Seletsky, A., O'Connell, M.R., Knight, S.C., Burstein, D., Cate, J.H.D., Tjian, R., and Doudna, J.A. (2016). Two distinct RNase activities of CRISPR-C2c2 enable guide-RNA processing and RNA detection. *Nature* 538, 270–273.
- East-Seletsky, A., O'Connell, M.R., Burstein, D., Knott, G.J., and Doudna, J.A. (2017). RNA targeting by functionally orthogonal type VI-A CRISPR-cas enzymes. *Mol. Cell* 66, 373–383.e3.
- Fierke, C.A., and Hammes, G.G. (1995). Transient kinetic approaches to enzyme mechanisms. *Methods Enzymol.* 249, 3–37.
- Fozouni, P., Son, S., Díaz de León Derby, M., Knott, G.J., Gray, C.N., D'Ambrosio, M.V., Zhao, C., Switz, N.A., Kumar, G.R., Stephens, S.I., et al. (2021). Amplification-free detection of SARS-CoV-2 with CRISPR-Cas13a and mobile phone microscopy. *Cell* 184, 323–333.e9.
- Fu, B.X.H., Smith, J.D., Fuchs, R.T., Mabuchi, M., Curcuru, J., Robb, G.B., and Fire, A.Z. (2019). Target-dependent nickase activities of the CRISPR-cas nucleases Cpf1 and Cas9. *Nat. Microbiol.* 4, 888–897.
- Fuchs, R.T., Curcuru, J., Mabuchi, M., Yourik, P., and Robb, G.B. (2019). Cas12a trans-cleavage can be modulated in vitro and is active on ssDNA, dsDNA, and RNA. *bioRxiv*, 600890. <https://doi.org/10.1101/600890>.
- Gong, S., Yu, H.H., Johnson, K.A., and Taylor, D.W. (2018). DNA unwinding is the primary determinant of CRISPR-cas9 activity. *Cell Rep.* 22, 359–371.
- Górecka, K.M., Krepl, M., Szlachcic, A., Poznański, J., Šponer, J., and Nowotny, M. (2019). RuvC uses dynamic probing of the Holliday junction to achieve sequence specificity and efficient resolution. *Nat. Commun.* 10, 4102.
- Hampton, H.G., Watson, B.N.J., and Fineran, P.C. (2020). The arms race between bacteria and their phage foes. *Nature* 577, 327–336.
- Holstein, C.A., Griffin, M., Hong, J., and Sampson, P.D. (2015). Statistical method for determining and comparing limits of detection of bioassays. *Anal. Chem.* 87, 9795–9801.
- Jeon, Y., Choi, Y.H., Jang, Y., Yu, J., Goo, J., Lee, G., Jeong, Y.K., Lee, S.H., Kim, I.S., Kim, J.S., et al. (2018). Direct observation of DNA target searching and cleavage by CRISPR-Cas12a. *Nat. Commun.* 9, 2777.
- Johnson, P.D.R., Stinear, T., Small, P.L.C., Plushke, G., Merritt, R.W., Portaels, F., Huygen, K., Hayman, J.A., and Asiedu, K. (2005). Buruli ulcer (M. ulcerans infection): new insights, new hope for disease control. *PLoS Med.* 2, 0282–0286.
- Knott, G.J., Thornton, B.W., Lobba, M.J., Liu, J.J., Al-Shayeb, B., Watters, K.E., and Doudna, J.A. (2019). Broad-spectrum enzymatic inhibition of CRISPR-Cas12a. *Nat. Struct. Mol. Biol.* 26, 315–321.
- Koonin, E.V., and Zhang, F. (2017). Coupling immunity and programmed cell suicide in prokaryotes: life-or-death choices. *BioEssays* 39, 1–9.
- Koonin, E.V., Makarova, K.S., and Zhang, F. (2017). Diversity, classification and evolution of CRISPR-Cas systems. *Curr. Opin. Microbiol.* 37, 67–78.
- Larremore, D.B., Wilder, B., Lester, E., Shehata, S., Burke, J.M., Hay, J.A., Milind, T., Mina, M.J., and Parker, R. (2020). Test sensitivity is secondary to frequency and turnaround time for COVID-19 surveillance. *medRxiv*. [Preprint]. 2020.06.22. 20136309. <https://doi.org/10.1101/2020.06.22.20136309>.
- Lee, R.A., de Puig, H., Nguyen, P.Q., Angenent-mari, N.M., Donghia, N.M., McGee, J.P., Dvorin, J.D., Klaperich, C.M., Pollock, N.R., and Collins, J.J. (2020). Ultrasensitive CRISPR-based diagnostic for field-applicable detection of Plasmodium species in symptomatic and asymptomatic malaria. *Proc. Natl. Acad. Sci. U S A*, 1–10.
- Li, J.J., Geyer, R., and Tan, W. (2000). Using molecular beacons as a sensitive fluorescence assay for enzymatic cleavage of single-stranded DNA. *Nucleic Acids Res.* 28, 52e–552.
- Li, S.-Y., Cheng, Q.-X., Wang, J.-M., Li, X.-Y., Zhang, Z.-L., Gao, S., Cao, R.-B., Zhao, G.-P., and Wang, J. (2018). CRISPR-Cas12a-assisted nucleic acid detection. *Cell Discov.* 4, 20.
- Li, Y., Li, S., Wang, J., and Liu, G. (2019). CRISPR/Cas systems towards next-generation biosensing. *Trends Biotechnol.* 37, 730–743.
- Liu, L., Li, X., Ma, J., Wang, M., Zhang, X., Wang, Y., Liu, L., Li, X., Ma, J., Li, Z., et al. (2017). The molecular architecture for RNA-guided RNA cleavage by Cas13a the molecular architecture for RNA-guided RNA cleavage by Cas13a. *Cell* 170, 714–720.e10.
- Marion, E., Ganlonon, L., Claco, E., Blanchard, S., Kempf, M., Adeye, A., and Chauty, A. (2014). Establishment of quantitative PCR (qPCR) and culture laboratory facilities in a field hospital in Benin: 1-year results. *J. Clin. Microbiol.* 52, 4398–4400.
- Meeske, A.J., Nakandakari-Higa, S., and Marraffini, L.A. (2019). Cas13-induced cellular dormancy prevents the rise of CRISPR-resistant bacteriophage. *Nature* 570, 241–245.
- Michaelis, L., and Menten, M. (1913). Die Kinetik der Invertinwirkung. *Biochem. Z.* 49, 333–369.
- Mo, C.Y., Mathai, J., Rostøl, J.T., Varble, A., Banh, D.V., and Marraffini, L.A. (2021). Type III-A CRISPR immunity promotes mutagenesis of staphylococci. *Nature* 592, 611–615.
- Modrich, P., and Zabel, D. (1976). EcoRI endonuclease physical and catalytic properties of the homogeneous enzyme. *J. Biol. Chem.* 251, 5866–5874.
- Moussaoui, M., Cuchillo, C.M., and Nogues, M.V. (2007). A phosphate-binding subsite in bovine pancreatic ribonuclease A can be converted into a very efficient catalytic site. *Protein Sci* 1, 99–109.
- Murugan, K., Seetharam, A., Severin, A., and Sashital, D. (2020). CRISPR-Cas12a has widespread off-target and dsDNA-nicking effects. *J. Biol. Chem.* 295, 5538–5553.
- Nouri, R., Tang, Z., Dong, M., Liu, T., Kshirsagar, A., and Guan, W. (2021). SCRISPR-based detection of SARS-CoV-2: a review from sample to result. *Biosens. Bioelectron.* 178, 113012.
- Phillips, R., Horsfield, C., Kuijper, S., Lartey, A., Tetteh, I., Nyamekye, B., Awuah, P., Nyarko, K.M., Lucas, S., Kolk, A.H.J., et al. (2005). Sensitivity of PCR targeting the IS2404 insertion sequence of Mycobacterium ulcerans in an assay using punch biopsy specimens for diagnosis of Buruli ulcer. *J. Clin. Microbiol.* 43, 3650–3656.
- Rehman, M.T., Dey, P., Hassan, M.I., Ahman, F., and Batra, J.K. (2011). Functional role of glutamine 28 and arginine 39 in double stranded RNA cleavage by human pancreatic ribonuclease. *PLoS ONE* 6, e17159. <https://doi.org/10.1371/journal.pone.0017159>.
- Shmakov, S., Abudayyeh, O.O., Makarova, K.S., Wolf, Y.I., Gootenberg, J.S., Semenova, E., Minakhin, L., Joung, J., Konermann, S., Severinov, K., et al. (2015). Discovery and functional characterization of diverse class 2 CRISPR-cas systems. *Mol. Cell* 60, 385–397.
- Siegmund, V., Adjei, O., Nitschke, J., Thompson, W., Klutse, E., Herberich, K.H., Thompson, R., van Vloten, F., Racz, P., Fleischer, B., et al. (2007). Dry reagent-based polymerase chain reaction compared with other laboratory methods available for the diagnosis of Buruli ulcer disease. *Clin. Infect. Dis.* 45, 68–75.
- Singh, D., Mallon, J., Poddar, A., Wang, Y., Tippana, R., Yang, O., Bailey, S., and Ha, T. (2018). Real-time observation of DNA target interrogation and product release by the RNA-guided endonuclease CRISPR Cpf1 (Cas12a). *Proc. Natl. Acad. Sci. U S A* 115, 5444–5449.
- Smargon, A.A., Cox, D.B.T., Pyzocha, N.K., Zheng, K., Slaymaker, I.M., Gootenberg, J.S., Abudayyeh, O.A., Essletzbichler, P., Shmakov, S., Makarova, K.S., et al. (2017). Cas13b is a type VI-B CRISPR-associated RNA-guided RNase differentially regulated by accessory proteins Csx27 and Csx28. *Mol. Cell* 65, 618–630.e7.
- Stella, S., Mesa, P., Thomsen, J., Moses, M.E., Hatzakis, N.S., Montoya, G., Jensen, S.B., Saligram, B., Moses, M.E., Hatzakis, N.S., et al. (2018). Conformational activation promotes CRISPR-cas12a catalysis and resetting of the endonuclease article conformational activation

promotes CRISPR-cas12a catalysis and resetting of the endonuclease activity. *Cell* 175, 1856–1871.

Sternberg, S.H., Redding, S., Jinek, M., Greene, E.C., and Doudna, J.A. (2014). DNA interrogation by the CRISPR RNA-guided endonuclease Cas9. *Nature* 507, 62–67.

Strohkendl, I., Saifuddin, F.A., Rybarski, J.R., Finkelstein, I.J., and Russell, R. (2018). Kinetic basis for DNA target specificity of CRISPR-cas12a. *Mol. Cell* 71, 1–9.

Swarts, D.C., van der Oost, J., and Jinek, M. (2017). Structural basis for guide RNA processing and seed-dependent DNA targeting by CRISPR-cas12a. *Mol. Cell* 66, 221–233.e4.

Tambe, A., East-Seletsky, A., Knott, G.J., Doudna, J.A., and O’Connell, M.R. (2018). RNA binding and HEPN-nuclease activation are decoupled in CRISPR-cas13a. *Cell Rep.* 24, 1025–1036.

Varble, A., and Marraffini, L.A. (2019). Three new Cs for CRISPR: collateral, communicate, cooperate. *Trends Genet.* 35, 446–456.

Wei, Y., Zhou, Y., Liu, Y., Ying, W., Lv, R., Zhao, Q., Zhou, H., Zuo, E., Sun, Y., Yang, H., et al. (2021). Indiscriminate ssDNA cleavage activity of CRISPR-Cas12a induces no detectable off-target effects in mouse embryos. *Protein Cell*, In press. <https://doi.org/10.1007/s13238-021-00824-z>.

Yan, W.X., Chong, S., Zhang, H., Makarova, K.S., Koonin, E.V., Cheng, D.R., Scott, D.A., Yan, W.X., Chong, S., Zhang, H., et al. (2018). Cas13d is a compact RNA-targeting type VI CRISPR effector positively modulated by a WYL-domain-containing accessory protein. *Mol. Cell* 70, 327–339.

Yan, W.X., Hunnewell, P., Alfonse, L.E., Carte, J.M., Keston-Smith, E., Sothiselvam, S., Garrity, A.J., Chong, S., Makarova, K.S., Koonin, E.V., et al. (2019). Functionally diverse

type V CRISPR-Cas systems. *Science* 363, 88–91.

Yang, W. (2011). Nucleases: diversity of structure, function and mechanism. *Q. Rev. Biophys.* 44, 1–93.

Yang, W., Lee, J.Y., and Nowotny, M. (2006). Making and breaking nucleic acids: two-Mg²⁺-ion catalysis and substrate specificity. *Mol. Cell* 22, 5–13.

Yotsu, R.R., Suzuki, K., Simmonds, R.E., Bedimo, R., Ablordey, A., Yeboah-Manu, D., Phillips, R., and Asiedu, K. (2018). Buruli ulcer: a review of the current knowledge. *Curr. Trop. Med. Rep.* 5, 247–256.

Zetsche, B., Gootenberg, J.S., Abudayyeh, O.O., Slaymaker, I.M., Makarova, K.S., Essletzbichler, P., Volz, S.E., Joung, J., Van Der Oost, J., Regev, A., et al. (2015). Cpf1 is a single RNA-guided endonuclease of a class 2 CRISPR-cas system. *Cell* 163, 759–771.

STAR★METHODS

KEY RESOURCES TABLE

REAGENT or RESOURCE	SOURCE	IDENTIFIER
Bacterial and virus strains		
<i>Mycobacterium ulcerans</i> NCTC 10417	ATCC	Cat#ATCC 19432
Biological samples		
Human skin swabs (Negative and positive for <i>M. ulcerans</i>)	Centre de Dépistage et de Traitement de l'Ulcère de Buruli, Pobè, Benin	https://ilepfederation.org/centre-de-depistage-et-de-traitement-de-la-lepre-et-de-lulcere-de-buruli-raoul-et-madeleine-follereau-de-pobe/
Human genomic DNA	Promega	Cat#G304A
Chemicals, peptides, and recombinant proteins		
LbCas12a	NEB	Cat#M0653T
Recombinant Cas12a from <i>Acidaminococcus</i> sp. BV3L6	IDT	AsCas12a
Recombinant Cas13a from <i>Leptotrichia buccalis</i> , wild-type	East-Seletsky et al., 2017	LbuCas13a
Recombinant Cas13a from <i>Leptotrichia buccalis</i> , processing mutant K1082A	East-Seletsky et al., 2017	LbuCas13a K1082A
DNase I	NEB	Cat#M0303S
RNase A	IDT	Cat#11-02-01-02
Dynabeads™ MyOne™ Streptavidin C1	ThermoFisher	Cat#65002
Critical commercial assays		
MagMAX™ Total Nucleic Acid Isolation Kit	ThermoFisher	Cat#AM1840
Qubit™ 1X dsDNA HS Assay Kit	ThermoFisher	Cat#Q33231
TaqMan Gene Expression Master Mix	Life Technologies	Cat# 4369106
Oligonucleotides		
ssRNA oligos	Synthego	See Table S1
DNA oligos	IDT	See Table S1
IS2404	IDT	See Table S1
RNaseAlert Substrate	IDT	Cat#11-04-03-03
DNaseAlert Substrate	IDT	Cat#11-04-03-04
Software and algorithms		
Prism 8	GraphPad	https://www.graphpad.com/
Excel	Microsoft	https://www.microsoft.com/

RESOURCE AVAILABILITY

Lead contact

Further information and requests for resources and reagents should be directed to and will be fulfilled by the lead contact, Damian Madan (damian.madan@ghlabs.org).

Material availability

This study did not generate new unique reagents.

Data and code availability

The published article includes all datasets generated or analyzed during this study.

EXPERIMENTAL MODELS AND SUBJECT DETAILS

Patient samples

Collection and use of human samples used in this study was approved by Le Ministre de la Santé, Bénin. Swabs were collected from open wounds of patients suspected of Buruli ulcer disease at Centre de Dépistage et de Traitement de l'Ulcère de Buruli, in Pobé, Bénin. At the field hospital collection site, swabs were rehydrated in 2.0 mL water, 400 μ L was processed for qPCR to ascertain presence of IS2404 as described (Marion et al., 2014), and the remaining sample was stored at -20°C.

METHOD DETAILS

Enzymes, RNA, and DNA

Recombinant LbCas12a and DNAase I were purchased from New England Biolabs (cat. no. M0653T, M0303S). Recombinant Cas12a from *Acidaminococcus* sp. BV3L6 (AsCas12a) was a gift from Integrated DNA Technologies (IDT). RNase A was purchased from IDT (cat. no. 11-02-01-02). Wild-type and crRNA-processing variant LbuCas13a were produced recombinantly and purified as described (East-Seletsky et al., 2017). RNA was purchased from Synthego. Synthetic DNA was purchased from IDT. IS2404 consists of a synthetic gBlock spanning 1299 bp of the repeat region present in *M. ulcerans*. RNaseAlert™ and DNaseAlert™ were purchased from IDT (cat. no. 11-04-03-03 and 11-04-03-04). Nucleic acid sequences are provided in Table S1. crRNA and the cognate targets they specify are designated by matching numbers: for example, the 20-nt spacer of crRNA-1 is complementary to the 20-nt protospacer of Target-1. Human genomic DNA was purchased from Promega (cat. no. G304A). Bacterial genomic DNA from *E. coli* and *M. ulcerans* NCTC 10417 (ATCC cat. no. 19432) was isolated using the MagMAX™ Total Nucleic Acid Isolation Kit (ThermoFisher, cat. no. AM1840) and quantified using the Qubit™ 1X dsDNA HS Assay Kit (ThermoFisher, cat. no. Q33231).

Substrate-capture and product quantification

Nuclease reactions described below were terminated by diluting reactions into a salt-EDTA quench solution composed of 1.0 M NaCl, 10 mM Tris-Cl, pH 7.5, 10 mM EDTA, and 0.01% Tween-20, unless otherwise indicated. Uncleaved biotin-labeled substrate was removed by addition of Dynabeads™ MyOne™ Streptavidin C1 (ThermoFisher Scientific, cat. no. 65002) diluted in salt-EDTA quench solution for at least 15 min at room temperature with end-over-end rocking. Bead quantities used in each reaction were scaled according to the amount of biotinylated substrate to be captured, based on the binding capacity of the beads (~500 pmol of ss oligo per mg of beads). Supernatants were removed from capture beads collected by magnetization and read on a BioTeK Synergy H1 fluorescence microplate reader at λ_{ex} 490 nm and λ_{em} 525 nm for Alexa Fluor™ 488 (Alexa488) and λ_{ex} 584 nm and λ_{em} 616 nm for Alexa Fluor™ 594 (Alexa594). When necessary, the concentration of product was calculated by converting fluorescence values (RFU) to molarity by comparison to linear standard curves of un-treated substrate performed in parallel.

Cas13a nuclease assays

Cleavage reactions were conducted in Cas13a assay buffer composed of 20 mM 4-(2-Hydroxyethyl)piperazine-1-ethanesulfonic acid (HEPES), pH 6.8, 50 mM KCl, 5.0 mM MgCl₂, 100 μ g/mL BSA, 0.01% Igepal CA-630, and 5% glycerol (East-Seletsky et al., 2017) in microtiter plates at final concentrations of reactants indicated (see Method Table). Assays performed in an alternative buffer lacking glycerol and KCl provided results qualitatively similar to the ones presented throughout this report; however, an approximately 10-fold reduction in catalytic efficiency for *trans*-cleavage of polyuridine and RNaseAlert by Cas13a activated by crRNA-Target-1 was observed (data not shown). For all experiments, 100 nM RNP was formed by incubating 200 nM Cas13a with 100 nM crRNA for at least 15 min at room temperature in buffer lacking Mg²⁺. Cleavage reactions were then performed at 37°C unless otherwise indicated. EDTA was pre-mixed with fluorescence substrates when testing the Mg²⁺-dependence of reactions. Reactions were terminated and processed as described above unless otherwise indicated.

In endpoint target-cleavage experiments (Figure 2A), RNP was incubated with dual fluorescent-biotin-labeled target DNA, and uncleaved substrate was removed by magnetic bead capture. In all endpoint *trans*-substrate cleavage experiments (Figures 2B, 3A–3C, S2, 6A, and 6B), RNP was incubated with unlabeled target RNA for at least 15 min at 37°C in buffer lacking Mg²⁺, then fluorescent *trans*-substrate was added in buffer containing Mg²⁺. For assays using dual fluorescent-biotin-labeled substrates (Figures 2B, 3A–3C, S2B–S2H, 6A, and 6B), uncleaved substrate was removed by magnetic bead capture. For assays

using RNaseAlert *trans*-substrate (Figure S2A), reactions were diluted into the salt-EDTA quench solution, and fluorescein fluorescence was recorded directly (λ_{ex} 490 nm and λ_{em} 525 nm).

In transient-state target-cleavage experiments (Figures 2C–2E, S3A, and S3B), RNP was mixed with fluorescent dsDNA target in buffer containing Mg^{2+} to initiate time courses. Control reactions, consisting of enzyme reactions lacking crRNA, were conducted in parallel. Transient-state experiments in which target and *trans*-substrate cleavage were measured simultaneously (Figures 2G and S3C) were conducted by mixing RNP with a solution containing a dual fluorescent-biotin-labeled RNA target (labeled with Alexa 488) and a dual fluorescent-biotin-labeled *trans*-substrate (labeled with Alexa 594) in a buffer containing Mg^{2+} to initiate time courses. Control reactions, consisting of enzyme reactions lacking crRNA, were conducted in parallel. At successive time points, cleavage reactions were terminated by dilution into the salt-EDTA quench solution or a denaturing solution containing 6.0 M guanidinium chloride and EDTA (Figure S3B) prior to removal of uncleaved substrate by magnetic bead capture.

In steady-state kinetics experiments (Figures 3D–3F, 3H, 3I, and S3D–S3K), RNP was incubated with RNA target in buffer lacking Mg^{2+} for at least 15 min, then mixed with varying amounts of fluorescent *trans*-substrate in buffer containing Mg^{2+} to initiate time courses, which were terminated by diluting reactions at successive time points into the salt-EDTA quench solution. Control reactions, consisting of enzyme reactions lacking crRNA, were conducted in parallel. Assays using dual fluorescent-biotin-labeled substrates (Figures 3D–3F, S3D, S3E, S3G, S3H, S3J, and S3K), uncleaved biotin-labeled *trans*-substrate was removed by magnetic bead capture. For cleavage of RNaseAlert *trans*-substrate (Figures 3H, 3I, S3F, and S3I), fluorescein fluorescence was measured continuously over several hours. When necessary, the concentration of cleaved product was determined by converting fluorescence values to molarity using a linear standard curve generated from the fluorescence values of cleavage reactions that had reached completion. The effect of tRNA was tested by including yeast tRNA (Sigma-Aldrich: cat. no. R5636) during the *trans*-cleavage phase of the reaction (Figure S3K).

Cas12a nuclease assays

Cleavage reactions were conducted in Cas12a assay buffer composed of 10 mM Tris-HCl, pH 7.5, 10 mM MgCl_2 , 1.0 mM Tris(2-carboxyethyl)phosphine hydrochloride, 50 $\mu\text{g}/\text{mL}$ BSA, and 0.01% Igepal CA-630 in microtiter plates at final concentrations of reactants indicated (see Method Table). Where indicated (Figures S4F and S4G), assays were performed in an alternative buffer composed of Cas12a assay buffer to which 5% glycerol and 100 mM KCl were included (Chen et al., 2017). For all experiments, 100 nM RNP was formed by incubating 100 or 200 nM Cas12a with 100 nM crRNA for at least 15 min at room temperature. Cleavage reactions were then performed at 37°C unless otherwise indicated. EDTA was pre-mixed with fluorescence substrates when testing the Mg^{2+} -dependence of reactions.

In endpoint target-cleavage experiments (Figure 4A), RNP was incubated with dual fluorescent-biotin-labeled target DNA, and uncleaved substrate was removed by magnetic bead capture. In all endpoint *trans*-substrate cleavage experiments (Figures 4B, 5A–5C, 6C–6H, S5, and S6), RNP was incubated with unlabeled target DNA for at least 15 min at 37°C, then fluorescent *trans*-substrate was added. For assays using dual fluorescent-biotin-labeled *trans*-substrates (Figures 4B, 5A–5C, 6C–6H, S5A, S5B, S5D, S5E, and S6), uncleaved substrate was removed by magnetic bead capture. Low and high concentrations of target tested in Figure 6C are 1.0 and 10 pM of IS2404 or 0.26 and 2.6 ng of genomic DNA: assuming 250 copies of IS2404 per genome (Phillips et al., 2005), these amounts of *M. ulcerans* contain 1.0 and 10 pM of protospacers in 20 μL reactions. For assays using DNaseAlert *trans*-substrate (Figure S5C), reactions were diluted into the salt-EDTA quench solution, and HEX fluorescence was recorded directly (λ_{ex} 535 nm and λ_{em} 563 nm).

In transient-state target-cleavage experiments (Figures 4C, 4D, S4A, and S4B), RNP was mixed with dual fluorescent-biotin-labeled dsDNA target to initiate time courses. Control reactions, consisting of reactions lacking crRNA (Figures 4C, 4D, and S4B) or RNP mixed with a solution of the target DNA containing EDTA (Figure S4A), were conducted in parallel. For transient-state experiments in which target and *trans*-substrate cleavage were measured simultaneously (Figure 4E), RNP was mixed with a solution containing a dual fluorescent-biotin-labeled dsDNA target (labeled with Alexa 488) and a dual fluorescent-biotin-labeled ssDNA *trans*-substrate (labeled with Alexa 594) to initiate time courses. For transient-state experiments in which cleavage of a dsDNA *trans*-substrate was measured (Figure 4F), RNP was mixed with a solution containing unlabeled dsDNA target and dual fluorescent-biotin-labeled non-target dsDNA

trans-substrate to initiate time courses. For both types of experiments, control reactions consisted of RNP mixed with a solution of targets and *trans*-substrates containing EDTA. At successive time points, cleavage reactions were terminated by dilution into a denaturing quench solution composed of 90% formamide and 20 mM EDTA prior to removal of uncleaved substrates by magnetic bead capture.

In steady-state kinetic experiments (Figures S5D–S5G and S4C–S4G), RNP was incubated with dsDNA target for at least 15 min, then mixed with varying amounts of fluorescent *trans*-substrate to initiate time courses. Control reactions, consisting of enzyme reactions lacking target DNA, were conducted in parallel unless indicated otherwise. For cleavage of dual fluorescent-biotin-labeled *trans*-substrates (Figures S5D, S5F, S5G, S4C, S4D, and S4F), time courses were terminated by diluting reactions at successive time points into the salt-EDTA quench solution prior to removal of uncleaved substrate by magnetic bead capture. For cleavage of the fluorescent dsDNA serving as both target and *trans*-substrate (Figure S5F), RNP was mixed with varying amounts of the fluorescent dsDNA to initiate time courses; control reactions, consisting of enzyme reactions lacking crRNA, were conducted in parallel. For cleavage of DNaseAlert *trans*-substrate, HEX fluorescence was measured continuously over several hours after initiation of time courses (Figures S5E and S4G) or after quenching at intervals with the salt-EDTA solution (Figure S4E), and cleaved product was quantified when need as described above for RNaseAlert reactions. The effect of heparin was tested by including sodium heparin (MP Biomedicals: cat. no 101931) during the *trans*-cleavage phase of the reaction (Figures S4F and S4G).

Fluorophore quantification and data analysis

Fluorescence readings of supernatants from which uncleaved substrates were removed by magnetic beads were compared to standard curves derived from titrations of starting solutions of fluorescent substrates to derive estimates of fluorophore concentrations (molarity). No adjustments were made to values to account for changes in fluorescence due to nuclease digestion of substrates (see below, Figure S1 and Table S2). Analytical limits of detection (LOD) and 95% confidence intervals were calculated using unweighted four-parameter logistic fit of raw fluorescence values of assay supernatants (Holstein et al., 2015) from selected experiments (Table S5).

In transient-state kinetic experiments, time-dependent changes in fluorescence reporter levels were processed as follows. Control fluorescence values collected in parallel were subtracted and converted to molarity, and the resulting values, $F(t)$, were subjected to ordinary least-squares fitting in GraphPad Prism v8.2 (GraphPad Software, Inc.). The single-exponential equation is given by:

$$F(t) = (F_0 - F_f) e^{-k_{obs}t} + F_f$$

where t is time, F_0 and F_f are initial and final fluorescent reporter values, respectively, and k_{obs} is the apparent first-order rate constant. The double-exponential (sequential) equation is given by:

$$F(t) = (F_0 - F_f) \left(1 - \left(\frac{k_{obs2}}{k_{obs2} - k_{obs1}} \right) e^{-k_{obs1}t} + \left(\frac{k_{obs1}}{k_{obs2} - k_{obs1}} \right) e^{-k_{obs2}t} \right) + F_f$$

where k_{obs1} and k_{obs2} represent the apparent first-order rate constants for the two sequential steps (Fierke and Hammes, 1995).

In steady-state kinetic experiments, linear fitting of control-corrected reporter values was performed to obtain initial velocities (V_0). Fitting of the substrate (S) dependence of V_0 to the hyperbolic Michaelis-Menten equation (Michaelis and Menten, 1913):

$$V_0 = V_{max} \left(\frac{[S]}{[S] + K_M} \right)$$

was performed to obtain V_{max} and Michaelis-Menten constant K_M . The constant k_{cat} was obtained by dividing V_{max} by the concentration of activated enzyme, which is given by the target concentration, assuming target is fully bound by RNP, an assumption validated in experiments in which RNP was increased four-fold (see Figure S3J for Cas13a and Figures S4C and S4D for Cas12a). In some cases, no approach to saturation was observed (e.g. U_5 and U_{10} cleavage by Cas13a activated by mature crRNA-Target-1 in Figure 3E), indicating $K_M \gg$ highest $[S]$ tested. In these cases, a lower limit estimate for K_M was set at the highest substrate concentration tested and linear fitting of the substrate-dependence of V_0 yielded slopes that, when divided by activated enzyme concentrations, yielded estimates for k_{cat}/K_M , and hence, k_{cat} . The

validity of all Cas13a *trans*-kinetic constants was corroborated by similarly analyzing rate data at low substrate concentrations (Table S4).

Steady-state kinetic constants were also estimated from endpoint experiments, as follows. For a given *trans*-substrate concentration, under conditions in which substrate conversion is low, V_0 is maintained throughout the experiment, and product increases linearly with time. Under such conditions, *trans*-product increases in direct proportion to target concentration (which serves as proxy for activated enzyme), and an apparent turnover rate (k_{app}) can be determined from the constant of proportionality (the slope) by taking into account the duration of the reaction. Since k_{app} represents $k_{cat} ([S]/([S] + K_M))$, k_{cat} and K_M may be estimated from the ratio of k_{app} calculated from two widely differing *trans*-substrate concentrations. For instance, for Cas12a activated by crRNA-Target-1 (Figure 5C, inset), k_{app} in the presence of 100 nM substrate C_{10} was $2.01 (\pm 0.02) s^{-1}$, which is less than ten times the value obtained using $1/10^{th}$ that concentration of substrate, which was $0.64 (\pm 0.02) s^{-1}$ for 10 nM C_{10} , suggesting the K_M value for C_{10} lies between 10 and 100 nM. Indeed, from the ratio of k_{app} values, an estimate of K_M equal to 31 nM is obtained, and, substituting this value back into the Michaelis-Menten equation, yields estimates for k_{cat} of $2.6 s^{-1}$ and k_{cat}/K_M of $8.4 \times 10^7 M^{-1} s^{-1}$, which agree reasonably well with steady-state analysis, which gave k_{cat} of $2.8 s^{-1}$, K_M of 28 nM and k_{cat}/K_M as $9.8 \times 10^7 M^{-1} s^{-1}$ (Table 1). For Cas13a activated by mature crRNA-Target-1, based on slope values, the k_{app} of $0.89 (\pm 0.01) s^{-1}$ for 100 nM U_{10} is approximately 10-times that in the presence of $1/10^{th}$ the concentration of *trans*-substrate, corresponding to $0.065 (\pm 0.001) s^{-1}$, using the crRNA-Target-1 pair (Figure 3A, inset). These results may be explained by an enzyme operating well below K_M , and assuming $K_M \gg 100$ nM (born out in steady-state analysis), k_{app} values suggest $k_{cat}/K_M > 7-9 \times 10^6 M^{-1} s^{-1}$ and $k_{cat} > 0.7 s^{-1}$, both consistent with steady-state analysis (Table 1). Similar analysis was performed for other Cas13a crRNA-target combinations (Figures 3B, 3C, and S2D–S2H; Table S3).

Nuclease digestion of nucleic acid reporter probes

Solutions containing 1.0 μM reporter nucleic acids and DNase I (4 units) or RNase A (0.02 milliunits) were incubated for 2 hr at 37°C in buffer composed of 10 mM Tris-HCl, pH 7.6, 2.5 mM MgCl₂, and 0.5 mM CaCl₂, or Cas13a assay buffer, respectively. Digests were then diluted into salt-EDTA quench solution, and fluorescence was recorded and normalized to that of untreated material (Figure S1 and Table S2). Since fluorescence output of DNase I-cleaved *trans*-substrate G₉C increases seven-fold (Table S2) and fluorescence signals were not corrected for this effect, product released using this substrate is likely overrepresented.

Creation of crRNA pools

A total of 21 crRNA designed against protospacers in hepatitis C viral RNA were tested individually with Cas13a on varying concentrations of their cognate target RNA and 100 nM *trans*-substrate U_{10} . Based on the resulting *trans*-RNase activities, 13 non-overlapping crRNA were chosen for pooling (Figure 6A), including crRNA-3 to -5, 1-2, 2-2, -6 to -10, 11-2, 12-2, and 13. *Trans*-activity of Cas13a bound with crRNA-3 or pooled crRNA (containing 77 pM of each crRNA) was tested on varied pooled target RNA (Figure 6B), consisting of equimolar concentrations of Target RNA-3 to -5, -1a, -2a, -6 to -10, -11, -12, and 13.

A total of 39 crRNA designed to target protospacers containing adjacent PAM sequences within IS2404 were tested individually with Cas12a on 10 pM IS2404 and *trans*-substrate C_{10} without pre-incubation of RNP and target (Figure 6E). Interference between equipotent pairs of Cas12a-crRNA complexes targeting adjacent or overlapping protospacers was investigated by measuring *trans*-activity of individual or paired crRNA (Figure S6), the results of which were interpreted as follows. If two different Cas12a-crRNA bind to and cleave target DNA at equal rates, then the resulting *trans*-activity of the paired crRNA should be at least 50% of the sum of individual activities, which was observed for every pair tested. If the two Cas12a-crRNA complexes act completely independently, then the resulting *trans*-activity of the pair should be 100% of the sum, which was observed for crRNA pairs targeting distantly separated protospacers. For interfering Cas12a-crRNA complexes, paired *trans*-activity will be considerably less than 100%, which was observed for complexes whose targeted footprints overlapped in a non-favorable relative orientation. The lower activity crRNA of an interfering pair was then excluded from consideration. Of the highest potency crRNA remaining, 20 were chosen for four sets of sub-pools (A – D), including crRNA-1 to -3, -5, and -7 to -22 (Figure 6E). Cumulative inclusion of sub-pools resulted in enhanced *trans*-activity that increased with diminishing magnitude reflecting the decreasing potency of the added sub-pools

(Figure 6F). Cas12a bound with 20 pooled crRNA containing each crRNA at 1/20th the total crRNA concentration was used for sensitive detection of IS2404 (Figures 6G and 6H).

Analysis of patient samples

Rehydrated swabs samples were shipped on dry ice prior to subsequent DNA extraction from 200 μ L of material using the QIAamp DNA Microbiome Kit (Qiagen, cat. no. 51704). The resulting DNA (50 μ L) was quantified by Qubit. qPCR with TaqMan Gene Expression Master Mix (Life Technologies cat. no. 4369106) using primers and probes specific for IS2404 (Table S1) was performed on 2.0 μ L of extracted material in triplicate using IS2404 as DNA standard (Figure 6H). *Trans*-activity of Cas12a was measured on 3.0 μ L of extracted material in triplicate in 20 μ L reactions composed of Cas12a, crRNA (pool of 20), *trans*-substrate C₂₀ in assay buffer supplemented with BSA (Figure 6H). Target DNA in samples was determined by interpolation to standard curves generated from a dilution series of IS2404 spanning 3.0–200 fM. From both qPCR and Cas12a, concentration of IS2404 is stated with reference to the 50 μ L extract.

QUANTIFICATION AND STATISTICAL ANALYSIS

Data in Figures 2, 3, 4, 5, 6, and S1–S6 were processed and visualized using Microsoft Excel and GraphPad Prism 8. The number of replicate wells analyzed for each data point in all experiment is indicated in the Method Table. The model used for least-squares fitting of data points in each experiment is indicated in figure legends and the procedures (see above).

Method table. Cleavage reaction conditions^a

Figure	Replicates	Cas (nM)	crRNA (nM)	Target	<i>Trans</i> -substrate (nM)	Time (hr)	Other (when indicated)
2A	3	5.0	2.5	1.0 nM	None	0.5	50 mM EDTA
2B	3	2.0	1.0	10 pM	100	1.0	25 mM EDTA
2C and 2D	2	Vary	Vary	1.0 nM	None	Vary	
2E	2	10	5.0	Vary	None	Vary	
2G and S3C	1	10	5.0	1.0 nM	Vary	Vary	
3A	3	2.0	1.0	Vary	10, 100	2.0	
3B and 3C	3	2.0	1.0	Vary	100	1.0	
3D–3F, S3D, S3E, S3G, and S3H	1	2.0	1.0	10 pM	Vary	Vary	
3H, 3I, S3F, and S3I	3	2.0	1.0	10 pM	Vary	Vary	
4A	3	5.0	2.5	1.0 nM	None	0.5	50 mM EDTA
4B and 6D	3	1.0	1.0	10 pM	100	1.0	50 mM EDTA
4C	2	Vary	Vary	1.0 nM	None	Vary	
4D	2	10	5.0	Vary	None	Vary	
4E	2	5.0	5.0	1.0 nM	Vary	Vary	
4F	2	5.0	5.0	1.0 nM	Vary	Vary	
5A, 5B, and 6C	3	1.0	1.0	Vary	100	2.0	
5C	3	1.0	1.0	Vary	10, 100	2.0	
5D	1	1.0	1.0	10 pM	Vary	Vary	
5E	3	1.0	1.0	10 pM	Vary	Vary	
5F	1	2.0	1.0	1.0 nM	Vary	Vary	
5G	1	2.0	2.0	1.0 nM	Vary	Vary	
6A and 6B	3	2.0	1.0	Vary	100	1.0	
6E and S6A	4–13	1.0	1.0	10 pM	100	1.0	
6F	3	1.0	1.0	10 pM	10	2.0	

(Continued on next page)

Continued

Method table. Cleavage reaction conditions^a

Figure	Replicates	Cas (nM)	crRNA (nM)	Target	Trans-substrate (nM)	Time (hr)	Other (when indicated)
6G	3	1.0	1.0	Vary	10	2.0	
6H	3	1.0	1.0	Vary	100	2.0	0.5 mg/mL BSA
S2A	3	2.0	1.0	100 pM	83	0.5	
S2B	3	1.0	0.5	500 pM	100	1.0	
S2C	3	2.0	1.0	10, 100 pM	100	2.0	
S2D–S2H	3	2.0	1.0	Vary	100	1.0	
S3A	3	5.0	2.5	1.0 nM	None	Vary	
S3B	3	Vary	Vary	1.0 nM	None	Vary	
S3J	1	8.0	4.0	10 pM	Vary	Vary	
S3K	1	2.0	1.0	100 pM	Vary	Vary	100 μg/mL yeast tRNA
S4A	3	5.0	5.0	1.0 nM	None	Vary	50 mM EDTA
S4B	3	10	5.0	1.0 nM	None	Vary	
S4C	1	1.0	1.0	10 pM	Vary	Vary	
S4D	1	4.0	4.0	10 pM	Vary	Vary	
S4E	1	1.0	1.0	100 pM	Vary	Vary	
S4F	1	5.0	6.26	100 pM	Vary	Vary	50 μg/mL heparin
S4G	3	5.0	6.25	100 pM	Vary	Vary	100 μg/mL heparin
S5A	3	1.0	1.0	2.5, 5.0, 10 pM	100	2.0	
S5B	3	1.0	1.0	Vary	100	0.5	
S5C	3	2.0	2.0	1.0 nM	83	0.25	
S5D	3	1.0	1.0	1.0 nM	100	1.0	50 mM EDTA
S5E	3	2.0	2.0	1.0 nM	100	1.0	50 mM EDTA
S6B and S6D	3	1.0	1.0	10 pM	100	1.0	

^a Cleavage reactions performed in the number of wells for each point in the indicated figures. Concentrations are given for the components during the cleavage phase of the reactions for the time indicated.